Wear 384–385 (2017) 28–42

Contents lists available at ScienceDirect

Wear

journal homepage: www.elsevier.com/locate/wear

Tribo-electrochemical behavior of bio-functionalized TiO_2 nanotubes in artificial saliva: Understanding of degradation mechanisms

Sofia A. Alves[a,b,*], André L. Rossi[c], Ana R. Ribeiro[b,d,e], Fatih Toptan[a,f], Ana M. Pinto[a,f], Jean-Pierre Celis[g,h], Tolou Shokuhfar[i,j], Luís A. Rocha[a,b,k]

[a] CMEMS – Center of MicroElectroMechanical Systems, Department of Mechanical Engineering, University of Minho, Azurém, 4800-058 Guimarães, Portugal
[b] IBTN/BR – Brazilian Branch of the Institute of Biomaterials, Tribocorrosion and Nanomedicine, Faculty of Sciences, UNESP – Universidade Estadual Paulista, 17033-360 Bauru, SP, Brazil
[c] Brazilian Center for Research in Physics, 22290-180 Rio de Janeiro, Brazil
[d] Directory of Life Sciences Applied Metrology, National Institute of Metrology, Quality and Technology, 25250-020 Duque de Caxias, RJ, Brazil
[e] Postgraduate Program in Translational Biomedicine, University of Grande Rio, 25070-000 Duque de Caxias, RJ, Brazil
[f] Department of Mechanical Engineering, University of Minho, Azurém, 4800-058 Guimarães, Portugal
[g] Department of Materials Engineering, KU Leuven, 3001 Leuven, Belgium
[h] Falex Tribology N.V., Wingepark 23B, 3110 Rotselaar, Belgium
[i] Department of Bioengineering, University of Illinois at Chicago, 60607 Chicago, IL, USA
[j] IBTN/US – American Branch of the Institute of Biomaterials, Tribocorrosion and Nanomedicine, University of Illinois at Chicago, 60612 Chicago, IL, USA
[k] Faculdade de Ciências, Departamento de Física, UNESP – Universidade Estadual Paulista, 17033-360 Bauru, SP, Brasil

ARTICLE INFO

Keywords:
TiO_2 nanotubes
Bio-functionalization
Film adhesion
Tribocorrosion
Dental implants

ABSTRACT

It has been shown that the synthesis of TiO_2 nanotubes by anodization provides outstanding properties to Ti surfaces intended for dental and orthopedic implants applications. Beyond the very well-known potential of these surfaces to improve osseointegration and avoid infection, the knowledge on the adhesion and degradation behavior of TiO_2 nanotubes under the simultaneous action of wear and corrosion is still poorly understood and these are issues of tremendous importance. The main aim of this work is to investigate, for the first time, the tribo-electrochemical degradation behavior of Ti surfaces decorated with TiO_2 nanotubes before and after bio-functionalization treatments.

Well-aligned TiO_2 nanotubes (NTs) were produced containing elements natively present in bone such as calcium (Ca) and phosphorous (P), in addition of zinc (Zn) as an antimicrobial agent and stimulator of bone formation. The synthesis of Ca/P/Zn-doped nanotubes (NT-Ca/P/Zn) was achieved by reverse polarization and anodization treatments applied to conventional TiO_2 nanotubes grown by two-step anodization. The nanotube surfaces were analyzed by scanning electron microscopy (SEM) while dark-field scanning transmission electron microscopy (STEM-DF) was used to characterize the Ti/TiO_2 nanotubular films interfaces. Tribo-electrochemical tests were conducted under reciprocating sliding conditions in artificial saliva. The open circuit potential (OCP) was monitored before, during and after sliding tests, and the coefficient of friction (COF) values were registered during rubbing action. The wear tracks resulting from sliding tests were characterized by SEM and wear volume measurements were carried out by 2D profilometry.

The results show that the tribo-electrochemical behavior of TiO_2 nanotubes was significantly improved after bio-functionalization treatments. The higher electrochemical stability and lower mechanical degradation of these films was correlated with their improved adhesion strength to Ti substrate, which is granted by the nano-thick oxide film formed at the interface region, during bio-functionalization processes. A first insight on the degradation mechanisms taking place during tribo-electrochemical action is proposed. The outcomes of this study may contribute in a great extent for the development of new implant surfaces with improved biomechanical stability and thus contribute for the long term success of dental implants.

* Corresponding author at: CMEMS – Center of MicroElectroMechanical Systems, Department of Mechanical Engineering, University of Minho, Azurém, 4800-058 Guimarães, Portugal.
E-mail addresses: sofiafonso@msn.com (S.A. Alves), tolou@uic.edu (T. Shokuhfar), lrocha@fc.unesp.br (L.A. Rocha).

http://dx.doi.org/10.1016/j.wear.2017.05.005
Received 13 February 2017; Received in revised form 7 May 2017; Accepted 12 May 2017
Available online 12 May 2017

1. Introduction

Titanium (Ti) and Ti alloys are the gold standard materials for dental implants applications mainly owing to their superior mechanical properties, biocompatibility and excellent corrosion resistance [1]. It is well documented that biocompatibility and corrosion resistance properties are mainly dictated by the formation of a well-adhering, dense and protective passive TiO_2 film (2–10 nm thickness) on the Ti-based materials surface when exposed to oxygen-containing environments [2–5]. However, despite the high corrosion resistance of Ti, the stability of the passive film may be modified in the presence of aggressive *in vivo* conditions, enhancing the corrosion process [6–9]. Furthermore, Ti-based materials display poor wear resistance, presenting severe adhesion wear and low abrasion resistance [9–12].

After implantation and the establishment of an adequate contact between bone and the implant surface (osseointegration), dental implants might be subjected to mechanical solicitations arising from biting forces generated during mastication. The masticatory action may induce cyclic micro-movements at the implant/bone interface and consequently to shear stresses at that place [9,13]. This occurs in the presence of a corrosive biological environment leading to the degradation of the dental implant material simultaneously by wear and corrosion processes, a phenomenon known as tribocorrosion [14–16]. As a consequence of wear-corrosion processes taking place at implant/bone interface, wear debris and corrosion products may be released to the implant surroundings and induce to adverse biological reactions and, ultimately, lead to implant loosening [17–19]. Various studies have been recently conducted to investigate the degradation of Ti-based implant materials by tribocorrosion processes [20–28]. In spite of the negative impact that tribocorrosion processes may have on the long term biological and mechanical stability of dental implants, the development of new implant systems addressing an integrated approach, which includes wear-corrosion resistance as a pre-requisite for implant success, is still lacking [29].

Recent advances in the fabrication of novel coatings and nanopatterning of dental implant surfaces have been achieved and there is a strong believe that nanoscale materials will produce the new generation of implant materials [30]. In the last decades, vertically aligned TiO_2 nanotubes grown in Ti surfaces by electrochemical anodization have become increasingly popular to enhance adhesion, growth and accelerate the osteogenic differentiation of osteoblasts and mesenchymal stem cells (MSCs) [31–36]. Furthermore, these nanostructures have shown the ability to display antimicrobial properties and thus inhibit microbial infections [37–45]. Additionally, TiO_2 nanotubes possess a lower elastic modulus (36–43 GPa) than cp-Ti (120–166 GPa), which is closer to that of natural bone (11–30 GPa), and thus TiO_2 nanotubular structured Ti surfaces are expected to have improved biomechanical compatibility, by reducing stress shielding effect [46–49].

TiO_2 nanotubes have been functionalized through different approaches in an attempt to develop new strategies for the construction of biomimetic systems mimicking the natural extracellular microenvironments, addressing osseointegration [33,50–52] and microbial implant-infection related issues [53,54]. Beyond all the evidences that TiO_2 nanotubes may effectively enhance cellular functions while simultaneously decrease bacterial action [55], the study of the adhesion properties of nanotubular films to the Ti substrate as well as their degradation mechanisms by wear-corrosion processes are still missing. These topics are of main relevance since poor adhesion strength of TiO_2 films before and/or after functionalization treatments, as well as their degradation through wear and corrosion mechanisms, may strongly compromise their use for osseointegrated implants applications. The biomechanical stability must be ensured after implantation since it might influence the implant lifetime, the probability of failure and thus the quality of life for implant receiving patients.

In this work the tribo-electrochemical degradation behavior of TiO_2 nanotubes before and after bio-functionalization processes is studied, for the first time, through reciprocating sliding tests in artificial saliva. A first insight on the tribo-electrochemical degradation mechanisms of TiO_2 nanotubes was proposed, and remarkable differences were observed between conventional and bio-functionalized TiO_2 nanotubes.

2. Experimental section

2.1. Surface pre-treatment

Commercially pure titanium (cp-Ti, ASTM grade 2) rod (McMaster-carr, IL, USA) was cut into discs of 15 mm diameter and 2 mm thickness. A series of silicon carbide (SiC) sandpapers from #240 to #1200 were used to ground cp-Ti disc surfaces followed by their polishing. The surface mirror finishing was achieved by using a polishing cloth with non-crystallizing colloidal silica suspension (MasterMet 2, Buehler, Lake Bluff, IL, USA). After polishing, the cp-Ti samples were cleaned in the ultrasonic bath in isopropanol (10 min) followed by distilled water (5 min), and finally dried at room temperature. Cp-Ti smooth surfaces were the substrates used in this study and were taken as the control group, named as Ti.

2.2. TiO_2 nanotubes synthesis and bio-functionalization

The synthesis of TiO_2 nanotubes relied on two-step anodization processes carried out in an organic electrolyte constituted of ethylene glycol (EG, Fluka Analytical, St. Louis, MO, USA), 0.3 wt% ammonium fluoride (NH_4F, Ammonium Fluoride, Sigma-Aldrich, St. Louis, MO, USA) and 3 vol% distilled water. The anodization processes were conducted at room temperature (22–24 °C) and the electrolyte was under continuous magnetic agitation (150 rpm). A DC power supply (Keysight (Agilent) Technologies N5772A) was used for the anodic treatments with a limiting current of 2.5 A.

For TiO_2 nanotube fabrication, firstly, Ti smooth samples (anode) were immersed in the EG electrolyte jointly with a graphite rod (cathode), separated at a distance of about 2 cm, and the power supply was set at 60 V for 1 h. Afterwards, the samples were ultrasonically cleaned in isopropanol (15 min) and distilled water (5 min) aiming to intentionally remove the nanotubular film grown in Ti surfaces during the first anodizing step, and create a nanopatterned Ti surface with nanotube bottom shape imprinted on it. Finally, these nanopatterned surfaces were anodized for 30 min at the previous conditions, to synthesize the TiO_2 nanotubular films with the desired morphology. At the end of the process, the samples were cleaned in isopropanol (10 min), distilled water (5 min) and dried at room temperature. The resulting Ti samples with TiO_2 nanotubes were named as NT.

The NT samples previously synthesized were bio-functionalized by following a new methodology described in a previous work [56], which relies on reverse polarization and anodization treatments. The processes were carried out in a continuously stirred (200 rpm) aqueous electrolyte composed of 0.35 M calcium acetate (Calcium acetate monohydrate, Sigma-Aldrich, St. Louis, MO, USA), 0.04 M β-glycerolphosphate (β-GP) (β-glycerolphosphate disodium salt pentahydrate, Sigma-Aldrich, St. Louis, MO, USA) and 0.35 M zinc acetate (Zinc acetate dihydrate, Sigma-Aldrich, St. Louis, MO, USA) as the source of Calcium (Ca), Phosphorous (P) and Zinc (Zn), respectively. The cathodic and anodic treatments were conducted at room temperature (22–24 °C) using a DC power supply (Keysight (Agilent) Technologies N5772A) set at a limiting current of 2.5 A. For bio-functionalization of TiO_2 nanotubes, the NT samples were immersed in the aqueous electrolyte containing Ca, P and Zn elements (Ca/P/Zn-based electrolyte), distanced 2 cm from a graphite rod. Afterwards, the samples were reverse polarized for 30 s, followed by anodization in the same electrolyte for 30 min at 100 V. Finally, the samples were cleaned in isopropanol (10 min), distilled water (5 min) and dried at room temperature. The resulting Ti samples decorated with Ca, P and Zn-doped TiO_2 nanotubes were named as NT-Ca/P/Zn. After preparation, the samples were stored

in a desiccator before performing tribocorrosion tests.

2.3. Surface and cross-section characterization of the TiO_2 nanotubular films

The surface morphology of TiO_2 nanotubular samples was investigated by scanning electron microscopy (SEM) using a JEOL JSM-6490LV. The surface chemistry of bio-functionalized nanotubes was accessed by energy-dispersive X-ray spectroscopy (EDS) (Pegasus X4M), using an acceleration voltage of 15 kV.

A dual beam instrument equipped with focused ion beam (FIB) with a gallium (Ga) ion source (TESCAN, LYRA 3) was used to obtain thin cross-sections (around 100 nm thick) of the TiO_2 nanotubular films. The samples surface was gold sputtered to improve the electrical conductivity during FIB preparation. To protect the thin cross-sections a platinum (Pt) layer of 1 μm was deposited in situ using a gas injection system and 1 nA Ga^+ ion current accelerated at 30 kV. Initial etching was conducted with 5 and 2 nA at 30 keV. Thinning was performed in 4 steps to obtain a lamella of ~100 nm: 1) 1 nA/30 keV; 2) 0.1 nA/10 keV; 3) 10 pA/5 keV; and 4) ~5 pA/3 keV. The cross-sections were observed at the Ti/TiO_2 nanotubes interface regions by dark-field scanning transmission electron microscopy (STEM-DF) using a JEOL 2100F operating at an accelerating voltage of 200 kV. The length of the nanotubular films was measured from the samples observed by STEM.

2.4. Tribo-electrochemical experiments

For tribo-electrochemical experiments, the different groups of samples were fixed in an electrochemical cell with the desired surface facing upwards and in contact with the electrolyte. A modified Fusayama's artificial saliva (AS) [57] was used at 37 °C (pH = 5.5), with chemical composition as follows: NaCl (0.4 g/L), KCl (0.4 g/L), $CaCl_2.2H_2O$ (0.795 g/L), $Na_2S.9H_2O$ (0.005 g/L), $NaH_2PO_4.2H_2O$ (0.69 g/L) and Urea (1 g/L). This electrolyte has been widely used in previous investigations [13,58–60] to simulate the highly corrosive oral cavity environment with Cl^-, F^-, and H^+ ions, playing a significant role on corrosion of dental implant materials [61]. Another reason for its use is related with the similar electrochemical behavior that metallic materials display in Fusayama´s saliva compared to the one in natural saliva [62]. The exposed surface area to AS was fixed at 0.63 cm^2.

The electrochemical cell was mounted on a CETR tribometer (Model UMT 2, Campbell, California, USA) in a pin-on-disk configuration, and an alumina (Al_2O_3) ball (Ø 10 mm) was selected as the counterbody material since it has high hardness, high wear resistance, chemical inertness and electrical insulating properties [9,63]. This material has been widely used as the counterbody in previously reported tribocorrosion studies, focused on osseointegrated implants applications [9,13,14,64–66]. A three-electrode setup was used with testing samples as the working electrode, a Pt counter electrode, and a saturated calomel electrode (SCE) (Hg/Hg_2Cl_2/saturated KCl solution; SCE = +244 mV *vs.* NHE) was used as the reference electrode.

For tribo-electrochemical experiments, the open circuit potential (OCP) was monitored prior to rubbing action until stabilization, during the whole duration of sliding and after the mechanical action, during 1800 s. The electrochemical measurements were carried out using a potentiostat Gamry Reference 600 coupled to Gamry framework software (Gamry Instruments, Warminster, PA, USA). To reproduce the daily mastication of a person, the reciprocating sliding tests against alumina ball were performed at a normal load of 1 N (initial Hertzian contact pressure of 400 MPa) and at a sliding frequency of 1 Hz for 1800 s [67,68]. Furthermore, a linear displacement amplitude of 650 μm was selected to simulate the micro-movements at implant-bone interface induced by the transmitted loads during mastication [68,69]. Moreover, additional tests were carried out for 300 s, aiming the better understanding of the tribo-electrochemical degradation mechanisms of the testing samples, as it is further on explained in more detail in the results and discussion sections. The tribometer was coupled to UMT-2 software (Campbell, California, USA) to monitor the tangential force during sliding, from which the friction coefficient (COF) was calculated. After testing, all the samples were ultrasonically cleaned with isopropanol during 10 min followed by distilled water for 5 min. Finally all the samples were dried at room temperature. It is noteworthy that all the experiments were performed for a minimum number of three samples for each condition, to assure the repeatability of the results.

2.5. Characterization of the wear tracks

After tribo-electrochemical experiments all the wear tracks were deeply analyzed. The morphological and chemical features of the wear scars were investigated by SEM (FEI Nova 200 (FEG/SEM)) and EDS (Pegasus X4M).

To calculate the volume of the degraded material from the samples exposed to tribo-electrochemical action (wear volume), the model previously described by Doni *et al.* [70] was followed. The wear track length was taken constant for all the tests as 650 μm, and the borders of the wear tracks were assumed as part of a calotte. The width and the deepness of the wear tracks were extracted from their profiles obtained by 2D profilometry (Veeco, Dektak 150) and the data analysis was performed with the aid of the affiliated software (Dektak version 9.4). For each wear track, three 2D profiles were taken in its central region. The final wear volume was calculated through the following equation:

$$\Delta V = \left[\frac{1}{3} * \pi * \overline{D}^2 (3R - \overline{D})\right] + \overline{A}_w * l \quad (1)$$

where ΔV is the total wear volume loss for each wear track in μm^3, $\overline{D}$ is the average deepness values, R is the radius of the alumina ball (counterbody), $\overline{A}_w$ is the average value of the wear loss area calculated from 2D profiles (obtained directly through the software), and l is the total length of the wear track (i.e. 650 μm). The final wear volume measurements were calculated from three wear tracks for each condition of test.

2.6. Statistical analysis

Data presented in this study are expressed as the arithmetic mean ± standard deviation (SD). The statistical tool SigmaStat 3.5 (Systat Software, San Jose, CA, USA) was used for statistical analysis. The evaluation of the data was carried out by one-way analysis of variance (ANOVA) in combination with Tukey HSD post hoc test for pair-wise comparisons between groups, with a significance level of $p < 0.05$.

3. Results

3.1. Characterization of TiO_2 nanotubular films

Titanium (Ti) smooth surfaces depicted in Fig. 1a were treated by two-step anodization in an ethylene glycol electrolyte containing fluoride (F^-) ions. Well-ordered Ti dioxide (TiO_2) nanotubes were grown from Ti surfaces, whose morphology is shown in Fig. 1b. The nanotubes are characterized by non-uniform diameters ranging from 50 to 90 nm as reported in a previous study [56]. The anodized Ti surfaces present a homogenous morphology, with TiO_2 nanotubular structures uniformly distributed along the surface area without film cracking. After bio-functionalization treatments by reverse polarization and anodization, zinc (Zn) was incorporated on nanotubular structures together with calcium (Ca) and phosphorous (P) without changing their surface morphology, as shown in Fig. 1c and d.

The cross-section of the nanotubular films, before and after bio-functionalization treatments, are shown in Fig. 2a and b respectively. Conventional anodic TiO_2 nanotubular films are characterized by a

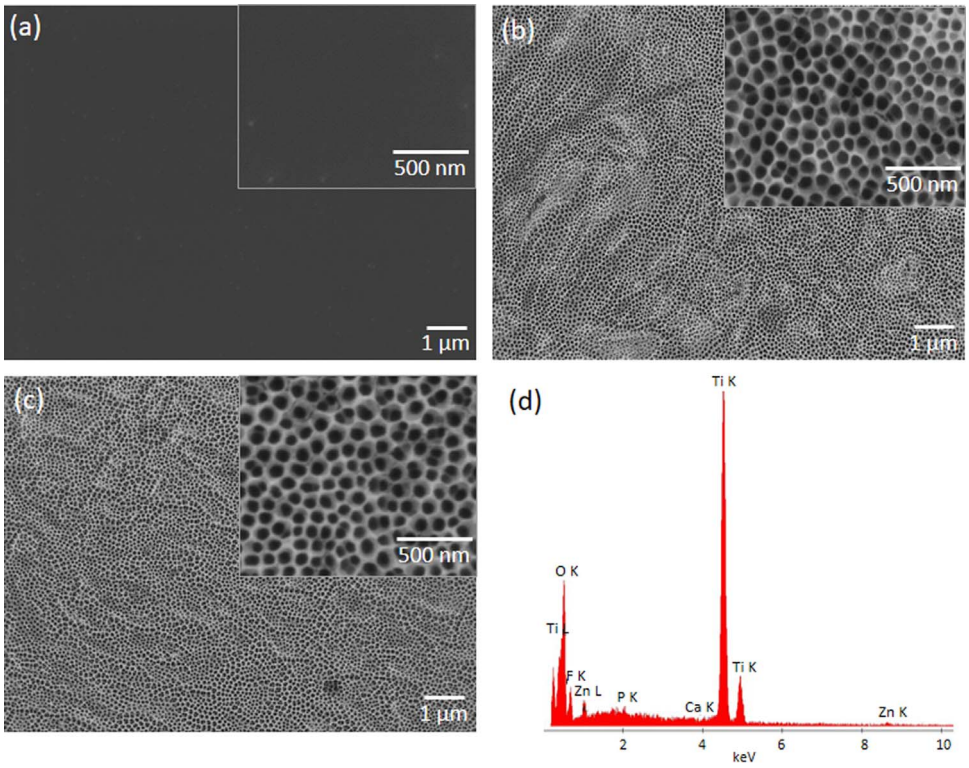

Fig. 1. SE SEM micrographs of (a) Ti, (b) NT and (c) NT-Ca/P/Zn surfaces. The inset images show the surface morphology in more detail. In (d) the EDS spectrum characteristic of NT-Ca/P/Zn samples is depicted.

non-continuous interface as observed in Fig. 2a. The presence of a hollow space between the film and the Ti substrate is observed suggesting a poor adhesion of the film. The interface of NT-Ca/P/Zn films present distinctive features as observed in Fig. 2b. This interface, beyond presenting some porosity at the nanoscale range, shows that the voided space existing before is not continuous anymore due to the formation of an oxide film during bio-functionalization treatments, with a thickness comprised between 230 and 250 nm.

3.2. Tribo-electrochemical behavior of TiO_2 nanotubular films

3.2.1. Electrochemical behavior before, during and after sliding

The evolution of the open circuit potential (OCP) before, during and after reciprocating sliding tests is shown in Fig. 3a. Before sliding Ti, NT and NT-Ca/P/Zn samples were immersed in artificial saliva (AS) and the OCP was recorded until stabilization. After the period of stabilization and before mechanical solicitations, the OCP of non-treated and Ti treated samples stabilized at different values, revealing their different tendencies to corrosion. As observed in Fig. 3a, NT-Ca/P/Zn samples display the highest OCP values (0.13 V *vs.* SCE) and so the lowest tendency to corrode, followed by NT (−0.15 V *vs.* SCE) and Ti smooth (−0.4 V *vs.* SCE) samples. The higher OCP values noticed for anodized Ti samples might be related with the presence of protective TiO_2 nanotubular films in their surfaces. The lower tendency to corrosion of TiO_2 nanotubes compared to Ti, has been already reported in previous studies [71,72]. The improved electrochemical behavior observed for TiO_2 nanotubes after bio-functionalization processes maybe ascribed to the protective nano-thick oxide film formed at the interface region, as it

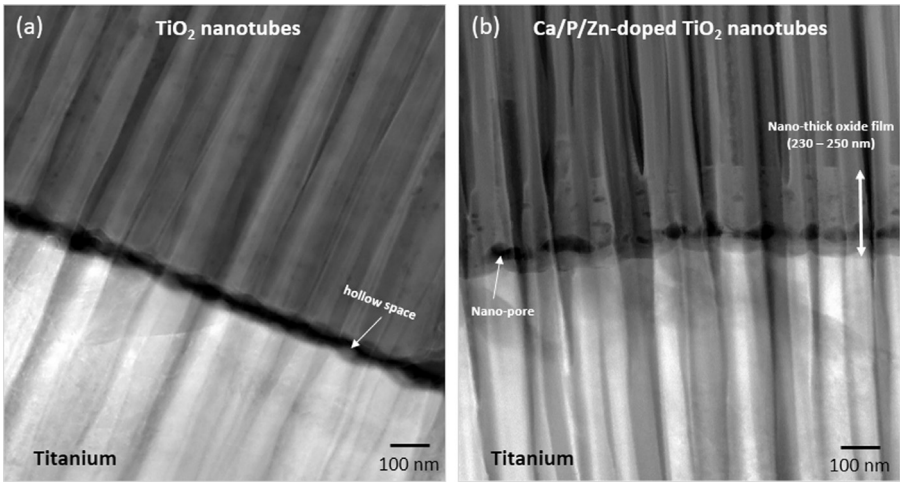

Fig. 2. STEM-DF micrographs of the FIB sections of (a) NT and (b) NT-Ca/P/Zn nanotubular films at the interface region. The inset white arrow in (a) highlights the hollow space existing between Ti substrate and NT film while in (b) shows the nano-pores existing at the interface instead of a continuous hollow space. In (b) is also depicted the nano-thick oxide film (230–250 nm) formed during bio-functionalization treatments.

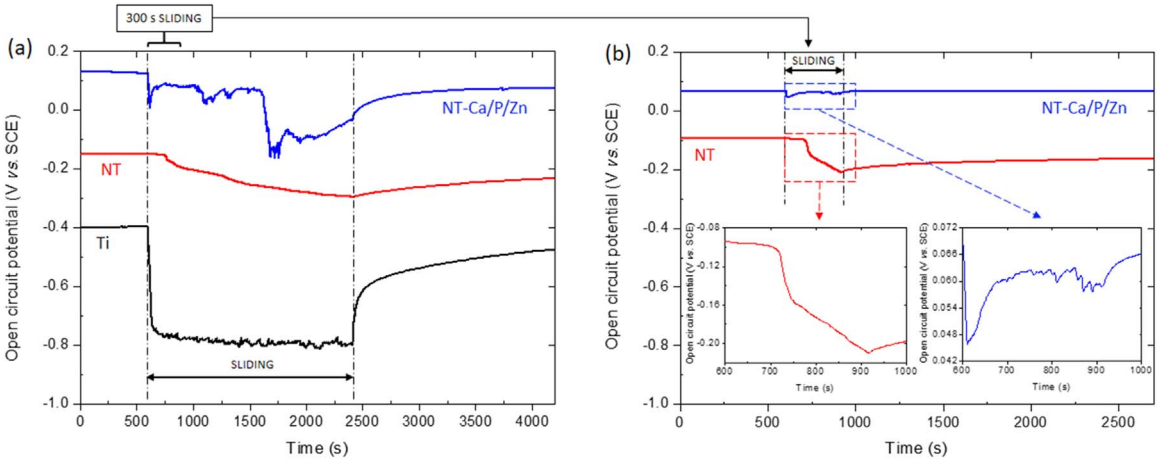

Fig. 3. Evolution of the open circuit potential (OCP) before, during and after reciprocating sliding tests in Ti, NT and NT-Ca/P/Zn samples during (a) 1800 s and (b) 300 s. The tribo-electrochemical experiments were performed in AS at a sliding frequency of 1 Hz, a load of 1 N and a displacement of 650 μm.

will be further on discussed in more detail. This trend is kept during the whole duration of sliding and also afterwards.

As soon as the mechanical solicitations start on Ti smooth samples a fast and significant potential drop is observed from −0.4 V *vs.* SCE down to approximately −0.8 V *vs.* SCE, indicating the quick disruption and/or removal of the TiO_2 native layer (depassivation) due to the rubbing action of the alumina counterbody [9]. Once Ti oxide film is mechanically depassivated, the bare Ti surface becomes in contact with fresh electrolyte and thus exposed to its corrosive effects, which causes a lowering in the OCP, whose final value is dependent on the surface ratio of passive-to-active material [73]. Small variations in the OCP values are observed during the whole duration of rubbing action, due to the successive depassivation/repassivation phenomena taking place in between mechanical contact events in the wear track. This depassivation/repassivation behavior of Ti immersed in AS was already reported by Souza *et al.* [13]. At the time sliding is finished, the OCP immediately evolves to higher values due to the progressive re-growth of the passive film (repassivation) in the wear track.

As soon as NT samples are submitted to rubbing action (Fig. 3a – red curve) the OCP is maintained stable for approximately 100 s and then a monotonic decrease takes place during the whole duration of sliding, reaching the lowest value of −0.3 V *vs.* SCE. This behavior suggests that during the first moments of sliding the TiO_2 nanotubes were able to withstand the mechanical action and protect the Ti substrate against corrosion. As soon as the mechanical interaction is stopped the OCP progressively and slowly evolves to higher values, revealing a gradual repassivation of the wear track. It is evident that after the period of stabilization, the OCP of NT samples reaches a lower value than the one initially recorded before sliding. This indicates that the electrochemical features in the worn area were changed after mechanical solicitations.

For NT-Ca/P/Zn samples a distinct behavior is observed compared to Ti and NT samples. As soon as the sliding starts the OCP drops and, immediately after, it goes back to noble values reaching a steady state for approximately 1000 s. After this plateau the OCP goes down until approximately −0.1 V and afterwards, it slightly evolves to higher values until the rubbing action is stopped. Once it is finished an uninterrupted repassivation occurs and at the end, the OCP reaches a stable and similar value to the one attained during the first plateau observed during the first 1000 s of sliding. For a better understanding of this behavior, additional reciprocating sliding tests were carried out for NT and NT-Ca/P/Zn samples for a shorter sliding period of 300 s. The OCP evolutions before, during and after the sliding tests carried out at this condition are depicted in Fig. 3b.

Considering NT samples, as soon as the sliding starts no significant potential variation is detected during approximately 100 s, as previously observed. After this period, the OCP drops gradually down until the end of rubbing action, as can be seen in more detail in the inset graph in Fig. 3b (red curve). Once the sliding is stopped the OCP tends to slightly increase and stabilize in a lower value than the one reached before sliding. This behavior demonstrates that a short period of mechanical solicitations on NT surfaces is enough to modify the electrochemical features of the worn area. A distinctive behavior is observed for NT-Ca/P/Zn surfaces. As depicted in more detail in the inset graph in Fig. 3b (blue curve), the mechanical solicitations leads to a decrease in the OCP followed by a fast recovery to higher values, after which a steady is reached. As the mechanical solicitations are stopped, the OCP goes back to the level before sliding, suggesting a complete recovery of the electrochemical properties of the film by repassivation in the wear track.

The evolution of the repassivation potential with time (repassivation kinetics) was calculated 300 s after the rubbing process was stopped, in accordance with the model reported by Hanawa *et al.* [74]. The repassivation kinetics was calculated using the following equation:

$$\Delta V = k_1 * log(t) + k_2 \quad (2)$$

where ΔV is the potential variation, t is the time after interrupting the sliding, k_1 represents the rate of repassivation and k_2 is a constant. These parameters were determined for sliding tests carried out for 1800 s, by fitting measured values to the Eq. (2). The repassivation kinetics is significantly higher ($p < 0.05$) for NT-Ca/P/Zn samples (0.046 ± 0.011 V/s) compared to NT samples (0.007 ± 0.002 V/s), which is in accordance with the significantly higher increase in the OCP after the end of sliding tests for bio-functionalized nanotubes (Fig. 3a – blue curve). As stated by Wood [15], the ability of a film to repassify quickly after its mechanical damage, is the key to being able to reduce the dissolution losses during wear-corrosion. As regards the repassivation rate of Ti samples (0.125 ± 0.01 V/s), it is significantly higher ($p < 0.001$) compared to both nanotubular samples.

3.2.2. *Coefficient of friction evolution during sliding*

The coefficient of friction (COF) evolution during sliding tests was recorded together with OCP and is shown in Fig. 4. For Ti smooth samples the COF was maintained relatively constant throughout the whole duration of sliding around a mean value of 0.5 (Fig. 4a). This is the expected value for the tribological pair Ti surface/alumina ball, as reported in previous studies [13,66]. Some oscillations are observed in the COF measured during sliding, which may be ascribed to the release of wear particles in the contact region (third body particles), with part of them being either accumulated or ejected out of the contact region as sliding keeps on [9,13].

Regarding NT samples, a short running-in-period is observed during

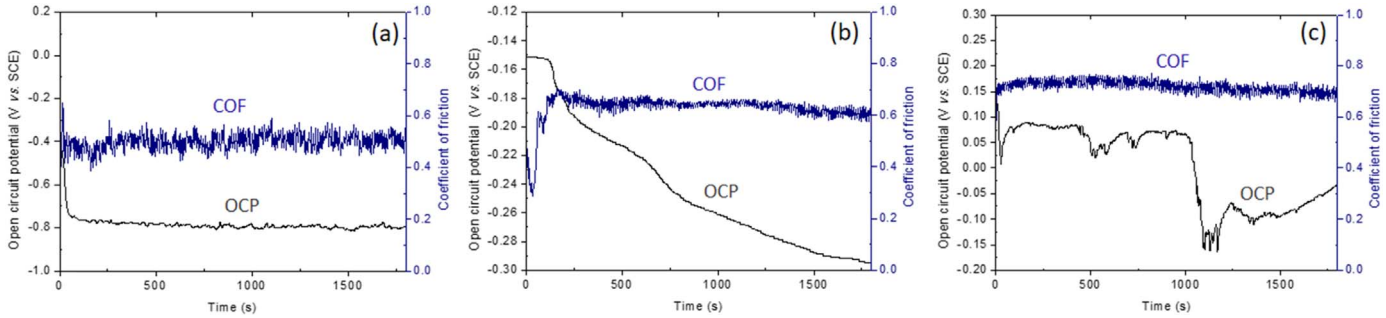

Fig. 4. Evolution of the open circuit potential (OCP) and the coefficient of friction (COF) during reciprocating sliding tests in (a) Ti, (b) NT and (c) NT-Ca/P/Zn samples during 1800 s. The tribo-electrochemical experiments were carried out in AS at a sliding frequency of 1 Hz, a load of 1 N and a displacement of 650 μm.

the first 100 s, which is related with the period during which the OCP is maintained stable (Fig. 4b). Afterwards, as long as the OCP progressively decreases, the COF is kept stable around a mean value of 0.65. However, approximately 600 s before the sliding is finished, the COF tends to slightly decrease to values near 0.6. On the NT-Ca/P/Zn samples no differences in the COF are noticed during the OCP plateau achieved in the first 1000 s of sliding, along which the values are kept constant around 0.75 (Fig. 4c). However, the decrease in the OCP values after this period, is accompanied by a slight decrease in the COF from 0.75 down to 0.70. These COF values indicate the presence of Ti oxide film in the worn area, since they are in accordance with the ones reported in literature for similar Ti oxide/alumina tribological pairs tested under similar conditions. Similar steady state COF values comprised between 0.6 and 0.8 were reported for reciprocating sliding tests carried out against alumina ball on anodized Ti samples [58,59,66].

3.2.3. Characterization of the wear tracks

The SEM micrographs representative of the wear tracks resulting from tribo-electrochemical tests are shown for Ti, NT and NT-Ca/P/Zn samples in Fig. 5a, b and c, respectively. The SEM images are shown both in secondary electrons (SE) and backscattered electrons (BSE) imaging modes, for a better understanding of the topographical and elemental features of the worn areas. The intensity of the BSE signal is related with the atomic number of the elements present in the sample since as higher the atomic number is, stronger the BSE signal. A region characterized by high atomic number elements is traduced in a brighter image and so, BSE images may provide important information on the elemental distribution along the wear tracks, with darker regions being related to the most oxidized areas (e.g. Ti oxides) once O has a lower atomic number than Ti.

The wear track morphology of Ti samples is shown in Fig. 5a, which presents curved borders, similar to the wear track morphology previously observed by Marques *et al.* [75] after reciprocating sliding tests on Ti immersed in AS with an alumina sphere. In Fig. 5b is clearly shown the irregular shape of the wear track of NT compared to Ti samples, as a result of nanotube film detachment from the Ti substrate. From BSE image, it is observed that a large part of the film was detached from the periphery of the contact area, since the brighter areas are correspondent to Ti substrate. This is an indicator of the poor adhesion of TiO_2 nanotubes to Ti. In the central area of this wear track, which corresponds to the sliding contact area, it is observed a darker region probably associated to wear debris resulting from film degradation, which have become entrapped and compacted generating a tribolayer. As observed in Fig. 5c the wear track on NT-Ca/P/Zn samples present huge differences compared to the one on NT samples. This wear track presents a completely different shape, with no signs of film detachment on its periphery. From BSE image it is observed that the film has been removed from the central part of the wear track (brighter areas), however, a large area is still protected with film. This is an indicator that bio-functionalized nanotubes display an improved ability to withstand cyclic mechanical solicitations avoiding film

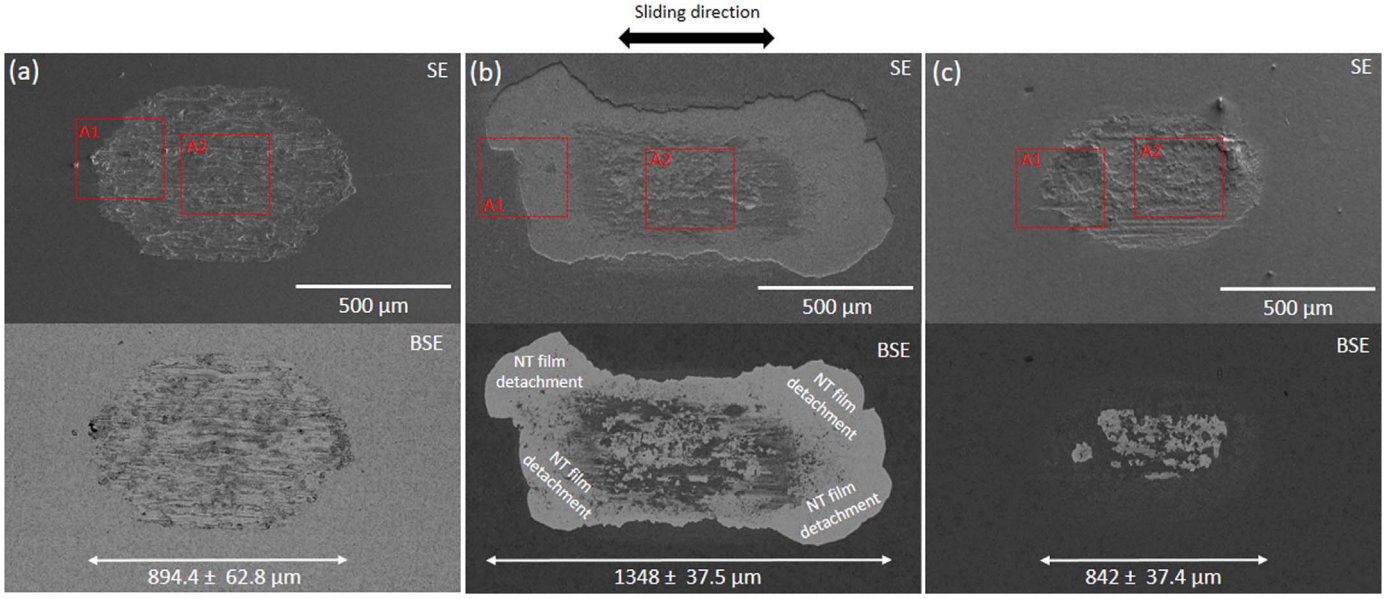

Fig. 5. SE/BSE SEM micrographs of the wear tracks resulting from tribo-electrochemical tests in (a) Ti, (b) NT and (c) NT-Ca/P/Zn samples for 1800 s of sliding duration. The maximum wear tracks length is included in BSE images for all the groups. The tribo-electrochemical experiments were carried out in AS at a sliding frequency of 1 Hz, a load of 1 N and a displacement of 650 μm.

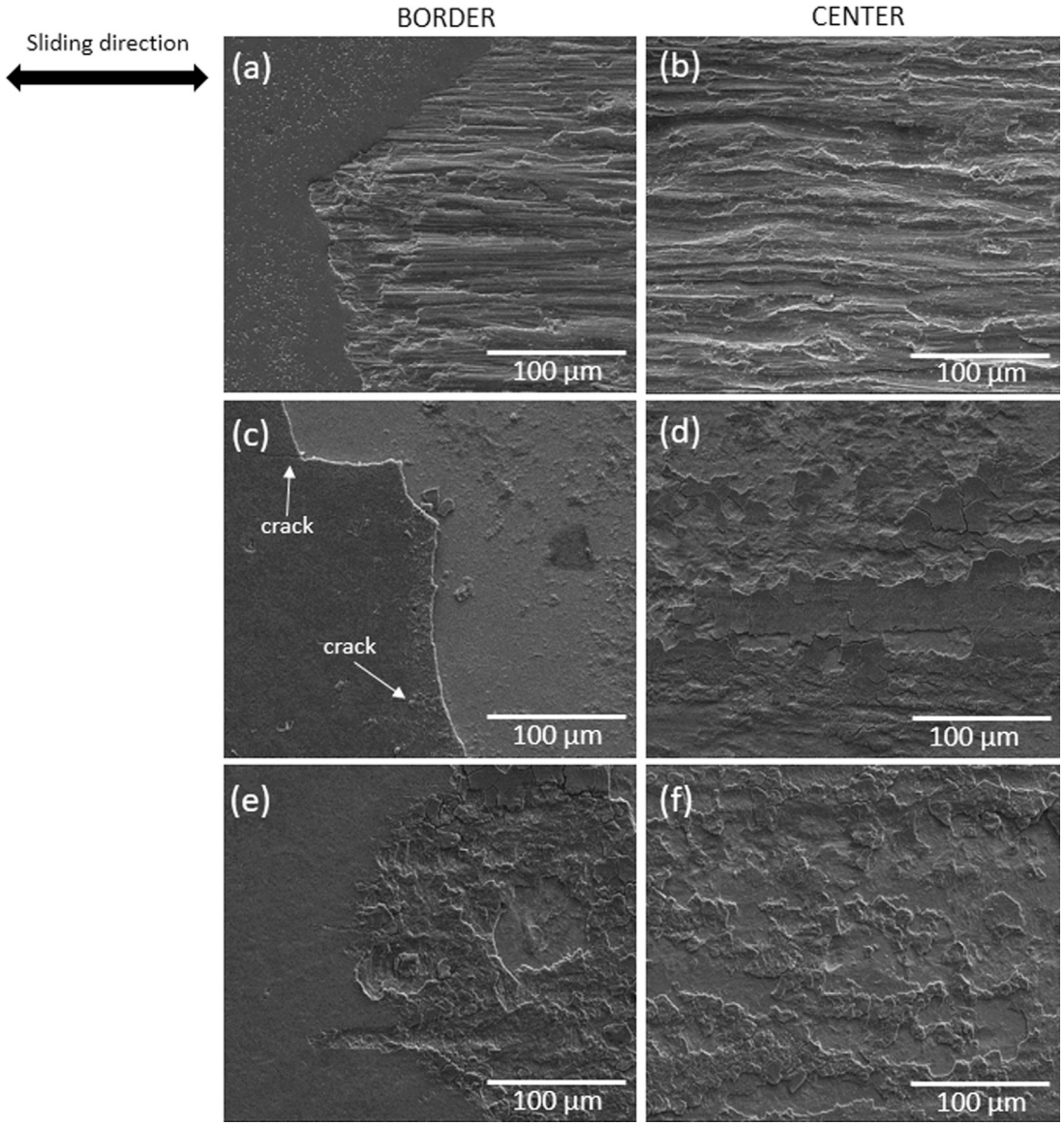

Fig. 6. SE SEM micrographs of the wear tracks of (a and b) Ti; (c and d) NT; (e and f) NT-Ca/P/Zn samples in the border and central regions. These are higher magnification images of the areas highlighted by the inset red squares in Fig. 5, named as A1 (border) and A2 (center). The tribo-electrochemical experiments were carried out in AS for 1800 s at a sliding frequency of 1 Hz, a load of 1 N and a displacement of 650 µm. (For interpretation of the references to color in this figure legend, the reader is referred to the web version of this article.)

detachment, probably due to the improved adhesion strength of bio-functionalized TiO_2 nanotubes to the Ti substrate. The higher mechanical destruction of NT samples is emphasized by their wear track length (1348 ± 37.5 µm), which is significantly higher ($p < 0.001$) compared to the maximum length measured on Ti (894.4 ± 62.8 µm) and NT-Ca/P/Zn (842 ± 37.4 µm) wear tracks.

Higher magnification SEM images were took in the border (A1) and in the central region (A2) of the wear tracks, as indicated by the inset red squares in Fig. 5a, b and c. These images are shown in Fig. 6. Regarding Ti samples (Fig. 6a and b), ploughing lines aligned in the direction of the sliding movement are observed probably resulting from third body particles entrapped in the contact region leading to a predominant abrasive wear mechanism. Furthermore, extensive plastic surface deformation is observed along the wear track resulting from the high and continuous contact pressure applied on the surface during rubbing with the harder ceramic counterbody [75].

As observed in Fig. 6c, the irregular border of the wear track of NT samples shows clear signs of film detachment. The presence of cracks are identified in the film outside the worn area, which might suggest film degradation by fatigue wear and film delamination. In the middle part of the worn area (Fig. 6d) severe plastic deformation and ploughing lines are observed in parallel to the direction of the counterbody movement showing evidences of abrasion. The wear debris coming out from film detachment may either act as abrasive bodies or get pressed between the two sliding bodies forming a compacted oxide layer between each other, as observed in Fig. 6d. As regards NT-Ca/P/Zn samples, abrasive wear marks are observed in SE image shown in Fig. 5c, along with plastic deformation of the nanotubular film (Fig. 6e and f). No signs of film detachment in the periphery of the wear track are observed, together with the absence of film cracking. For all the samples, mechanical wear also occurred by adhesion phenomena, through material transfer from the materials surface to the alumina ball, as observed under naked eyes after sliding tests. Wear of anodized Ti samples by abrasion and adhesion mechanisms have been previously identified in other studies [14,65,75].

Detailed SEM micrographs in the border and central regions of the wear tracks are shown in Fig. 7 for NT and NT-Ca/P/Zn samples. From BSE images shown in Fig. 7a is clear the entire detachment of TiO_2 nanotubes from the periphery of the sliding contact area. In the central region of the wear track (Fig. 7b) it is observed part of the compacted

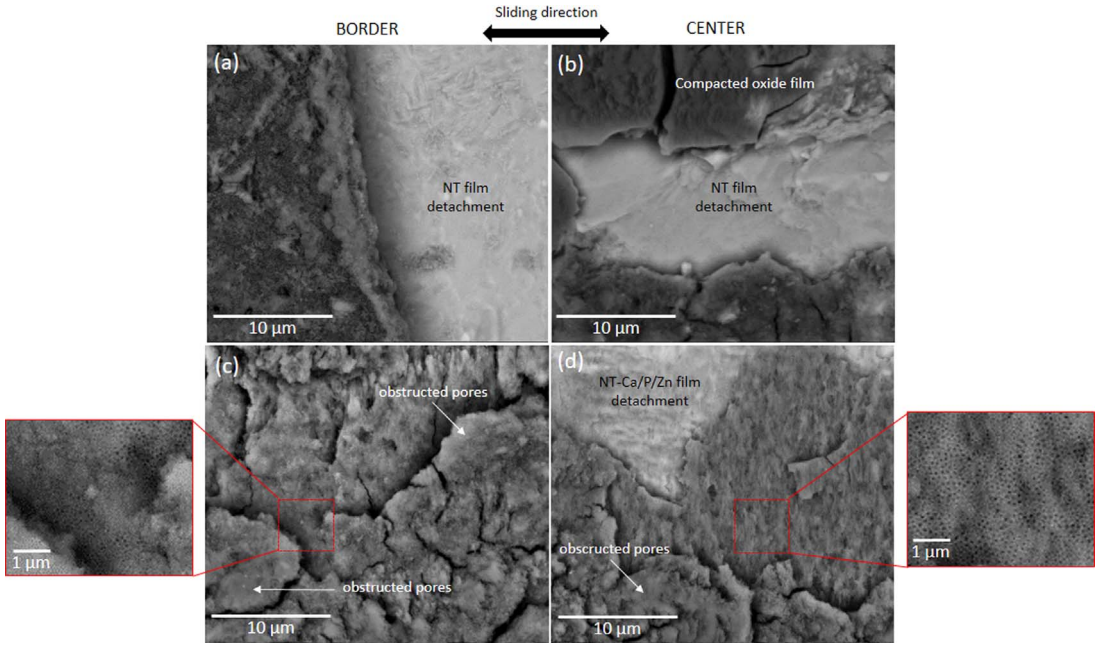

Fig. 7. BSE SEM micrographs of the wear tracks of (a and b) NT; (c and d) NT-Ca/P/Zn samples in the border and central regions. The inset images in (c) and (d) show that TiO_2 nanotubes survived both in the border and central regions of the worn NT-Ca/P/Zn samples. The tribo-electrochemical experiments were carried out in AS for 1800 s at a sliding frequency of 1 Hz, a load of 1 N and a displacement of 650 µm.

oxide film (darker region) and the Ti substrate in the underlying plan (brighter region). From higher magnification images took in the border of the wear track of NT-Ca/P/Zn samples (Fig. 7c) is observed that the film is organized in different layers, which are structured in different plans. No signs of complete detachment of the film is found in this region, and interestingly, it is observed that the nanotubes still maintain their integrity in the subsurface plans (inset image in Fig. 7c). In the uppermost part of the film it seems that the wear debris became entrapped in the open pores of the nanotubes filling them up and, in some cases, covering the nanoporous structure. The wear track in the central region (Fig. 7d) presents similar characteristics with nanotube structures obstructed in the outermost part of the film, and remaining undamaged in the underlying plans (inset image in Fig. 7d). From BSE image it is evident that the nanotubular film detached from specific areas, as highlighted in the figure.

The elemental composition of the wear tracks was investigated. EDS spectra were acquired from two different regions, the less oxidized (brighter areas – A1) and the most oxidized (darker areas – A2), as depicted in Fig. 8a and b for NT and NT-Ca/P/Zn wear tracks, respectively. From Fig. 8a it is confirmed both the presence of Ti in the brighter areas and the presence of Ti oxide in the darker ones. Elements present in the electrolyte such as P, potassium (K) and Ca were also detected in the oxidized regions. The same observations were found for NT-Ca/P/Zn wear tracks. In this case, the detection of Ca and P elements may be also related with the composition of NT-Ca/P/Zn films.

In Fig. 9a and b the wear tracks of NT and NT-Ca/P/Zn samples resulting from 300 s sliding tests are shown, respectively. After 300 s of mechanical solicitations, the non-functionalized TiO_2 nanotubes detached from the contact region and neighboring areas, with part of the oxide film remaining in the central region of the wear track, as depicted in SE and BSE images in Fig. 9c, which are amplified from the inset red square in Fig. 9a. Scratches/grooves along with severe plastic deformation are visible inside the wear track aligned with the pin movement. From Fig. 9b it can be seen that bio-functionalized TiO_2 nanotubes present significantly lower mechanical damage with no signs of film detachment, as evident from higher magnification images shown in Fig. 9d.

3.2.4. Wear volume and wear track profiles

Wear volume measurements were carried out based on 2D profiles extracted from the central region of the wear tracks by 2D profilometry. The wear volumes calculated for all the groups of samples submitted to sliding tests during 1800 s and 300 s are shown in Fig. 10. The wear volume estimated from wear scar dimensions is the sum of wear loss due to corrosion and the wear loss due to sliding wear [65]. After tribo-electrochemical tests carried out for 1800 s, the wear volume of NT samples was $2.9 \pm 0.4 \times 10^6$ µm^3, significantly higher compared to Ti ($1.9 \pm 0.3 \times 10^6$ µm^3) and NT-Ca/P/Zn ($1.2 \pm 0.2 \times 10^6$ µm^3) samples. Similar results were acquired for sliding tests performed during 300 s, with NT samples presenting a significantly higher wear volume ($3.2 \pm 0.8 \times 10^6$ µm^3) compared to NT-Ca/P/Zn samples ($0.5 \pm 0.4 \times 10^6$ µm^3). These calculated wear volumes show similarities to the ones reported in literature. For example, Alves *et al.* [59] reported a wear volume of around 2×10^7 µm^3 and 2.5×10^6 µm^3, estimated from confocal microscopy, for tribocorrosion of non-treated and anodic treated Ti samples, respectively. Furthermore, Oliveira *et al.* [14] calculated the wear volume of Ti samples by 3D profilometry as $96.5 \pm 2.1 \times 10^6$ µm^3, after tribocorrosion testing. The existing differences are probably related with the different parameters of test used, which were more aggressive than the ones selected in this work, therefore inducing to higher wear volume values.

The 2D profiles representative of the wear tracks remaining on Ti, NT and NT-Ca/P/Zn samples after 1800 s sliding tests are depicted in Fig. 11a, while in Fig. 11b are shown the wear tracks profiles on NT and NT-Ca/P/Zn samples submitted to 300 s sliding tests. The maximum depth reached in the wear tracks is depicted in Table 1, jointly with the film thickness values for each different group of samples. The wear scar depth of Ti samples achieved a maximum value around 10.7 ± 0.4 µm, which is significantly higher than the ones measured on NT (7.9 ± 0.9 µm) and NT-Ca/P/Zn (7.1 ± 0.4 µm) samples. The maximum wear track depths measured on nanotubular samples are in the same order of magnitude of the films thickness (Table 1), indicating that in both cases the films were fully detached from the substrate. For sliding tests carried out for 300 s, the maximum depth of the wear track on NT samples (8.3 ± 1.2 µm) is significantly higher compared to NT-Ca/P/Zn samples (4.1 ± 0.1 µm) as clearly observed in Fig. 11b, which is in accordance with the significant lower wear volume measured for

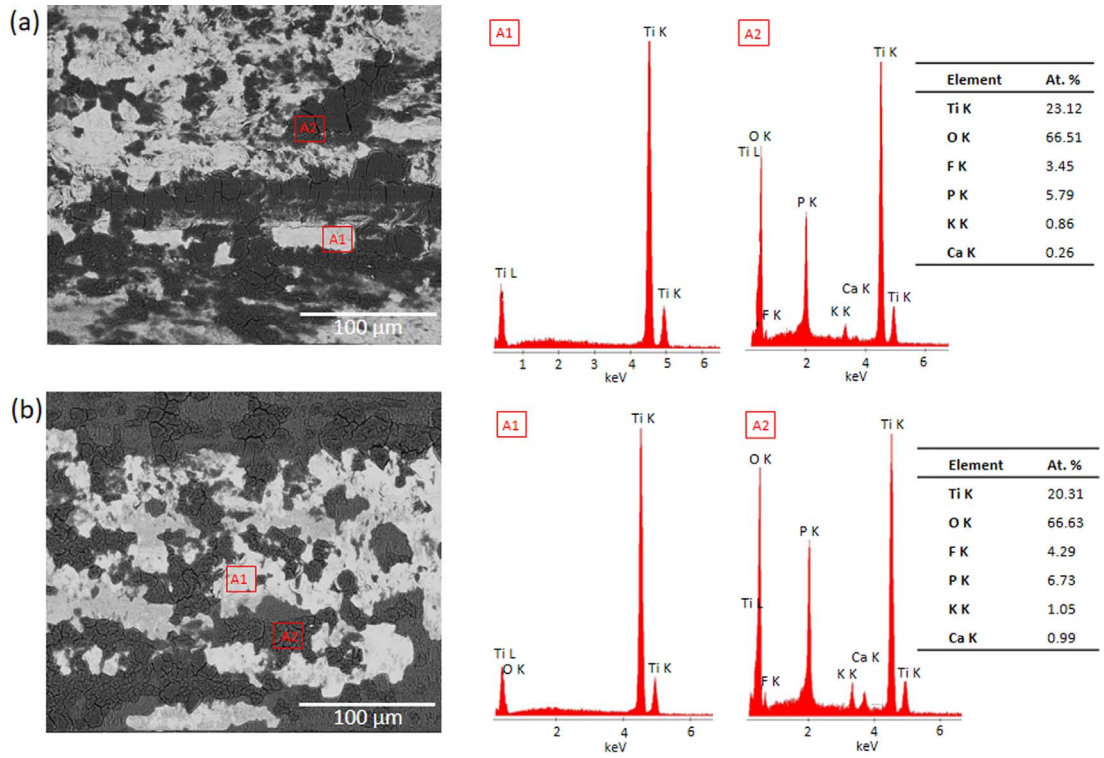

Fig. 8. BSE SEM micrographs in the central region of the wear tracks of (a) NT and (b) NT-Ca/P/Zn surfaces. The EDS spectra acquired from the inset squares (A1 and A2) are shown for both groups, together with the description of the chemical elements found and their atomic percentages (At%). The tribo-electrochemical experiments were carried out in AS for 1800 s at a sliding frequency of 1 Hz, a load of 1 N and a displacement of 650 µm.

bio-functionalized samples.

4. Discussion

4.1. Surface and interfacial features of TiO_2 nanotubular films

TiO_2 nanotubes were grown from Ti smooth surfaces presenting a bone-inspired morphology at a nanoscale (Fig. 1b). The well-ordered structure of the nanoarrays was achieved by two-step anodization of Ti in an organic electrolyte containing fluoride (F^-) ions. This methodology allows the synthesis of well-aligned nanotubular films with a specific morphology, which is preset by the first anodization step through the production of hemispherical footprints on Ti smooth surfaces. The mechanisms underlying the nanotube formation by two-step anodization in a fluoride containing electrolyte are well documented in literature [76–79]. The methodology to acquire the specific surface morphology depicted in Fig. 1b is reported in detail in a previous study [56], in which the mechanisms underlying nanotube formation are addressed and established a correlation with the final surface morphology achieved.

Beyond the morphology, the surface chemistry is also known to play a crucial role on cellular functions [80]. The doping of TiO_2 nanotubes with Ca and P elements natively present in bone, together with Zn, which is known to induce osteogenic differentiation and provide antibacterial activity [55], was successfully achieved by reverse polarization and anodization treatments of NT samples in a Ca/P/Zn-based electrolyte. The bio-functionalization treatments were applied without compromise the surface morphology previously achieved, as shown in Fig. 1c. Dissimilar features are found at the Ti/TiO_2 nanotubes interface before and after bio-functionalization treatments, as revealed in Fig. 2a and b, respectively. As a consequence of reverse polarization anodization of conventional TiO_2 nanotubes, the growth of a nano-thick oxide film (230–250 nm) takes place at the interface region, which appears to improve the adhesion of the nanotubular film to Ti substrate. Probably, by applying an anodic voltage of 100 V to TiO_2 nanotubular samples in the Ca/P/Zn-based electrolyte, Ti^{4+} ions liberated as a consequence of anodic polarization of Ti react with O^{2-} ions present in solution, and moving in the opposite direction under the action of the electric field, leading to the formation of the Ti oxide film at the interface region [76]. However, further studies must be performed to validate this hypothesis. The features of Ti/TiO_2 nanotubes interface may influence the biomechanical stability of the film and thus the ability to withstand cyclic mechanical solicitations, which may compromise its long term success for osseointegrated implant applications. Beyond the wide range of studies reported in literature showing the promising features of TiO_2 nanotubes, most of them are concerned with their impact on biological performances. No information regarding the degradation behavior of the nanotubular systems by the simultaneous action of wear and corrosion is reported, which is a subject of paramount importance. The understanding of the tribo-electrochemical behavior of TiO_2 nanotubes before and after bio-functionalization treatments is the main aim of this work, and is addressed in the following section.

4.2. Tribo-electrochemical degradation mechanisms of TiO_2 nanotubes before and after bio-functionalization treatments

After immersion of Ti, NT and NT-Ca/P/Zn samples in AS, and before sliding tests, their OCP stabilized at different values, reflecting different surface activation stages (Fig. 3a). As reported by Ponthiaux *et al.* [16] the OCP provides information on the electrochemical state of a material, reflecting its active or passive state. An increase in the OCP (anodic shift) indicates a more passive state and on the contrary, a decrease (cathodic shift) indicates a more active state. After the period of OCP stabilization, a dense and passive oxide film of a few nanometers is expected to be present on Ti smooth surfaces [71,81], while micron-length TiO_2 nanotubular films exist in both anodized Ti surfaces. The higher OCP achieved for NT and NT-Ca/P/Zn samples (Fig. 3a) may be associated to the physical barrier created by TiO_2 nanotubular films with insulating properties. The less active state of TiO_2 nanotubes in

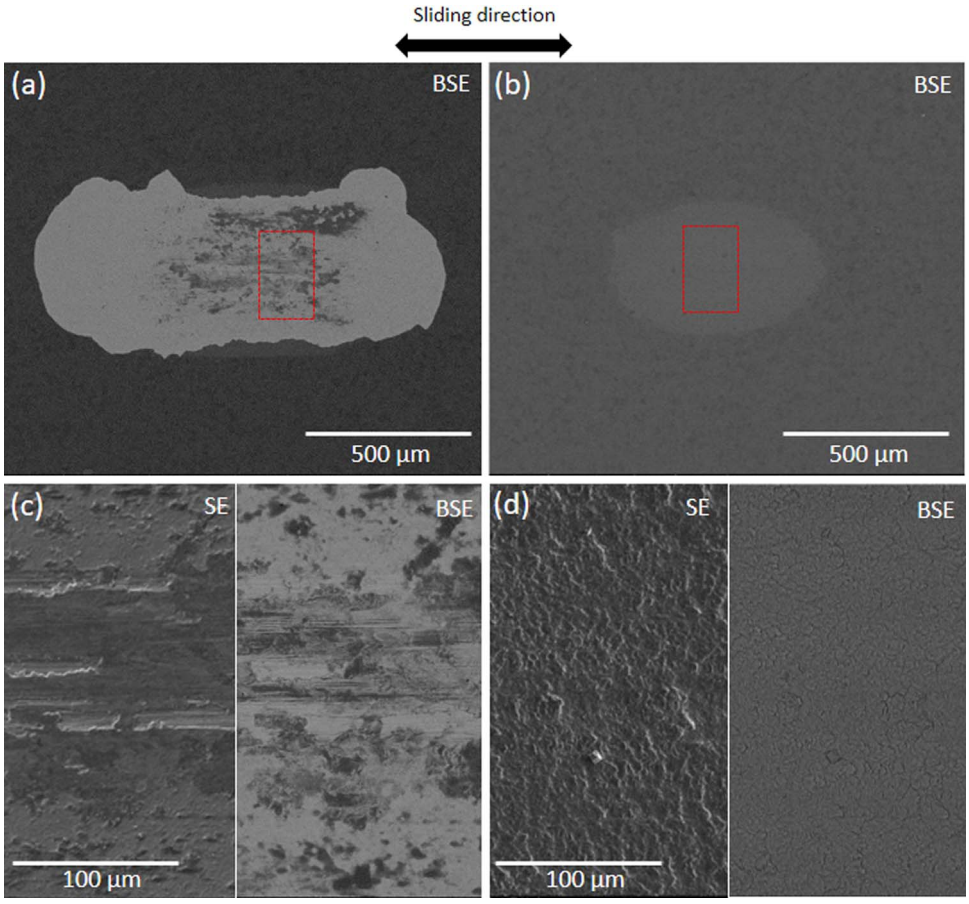

Fig. 9. BSE SEM micrographs of the wear tracks of (a) NT and (b) NT-Ca/P/Zn samples after 300 s of sliding. Higher magnification SE/BSE SEM images were obtained from the inset red squares and are shown in (c) for NT and in (d) for NT-Ca/P/Zn surfaces. The tribo-electrochemical experiments were carried out in AS at a sliding frequency of 1 Hz, a load of 1 N and a displacement of 650 µm. (For interpretation of the references to color in this figure legend, the reader is referred to the web version of this article.)

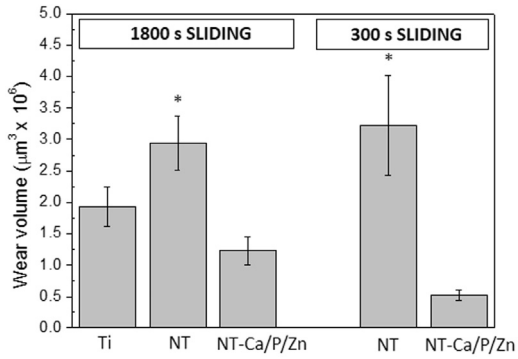

Fig. 10. Wear volume measurements after tribo-electrochemical tests carried out for 1800 s and 300 s sliding tests. For 1800 s SLIDING: (*) significantly different from Ti and NT-Ca/P/Zn, $p < 0.05$; for 300 s SLIDING: (*) significantly different from NT-Ca/P/Zn, $p < 0.001$. The tribo-electrochemical experiments were carried out in AS at a sliding frequency of 1 Hz, a load of 1 N and a displacement of 650 µm.

different simulating body fluids has been reported in previous works [3,71,72,82].

The fast and effective passivation behavior of NT samples was demonstrated in our previous study by potentiodynamic polarization studies in AS [56]. Demetrescu *et al.* [3] concluded that the low corrosion current density obtained for the TiO_2 nanotube samples tested in AS, was correlated to the formation of a strong passive barrier layer. Furthermore, Yu *et al.* [71,72] demonstrated that TiO_2 nanotubes display better corrosion resistance compared to smooth Ti, which was also ascribed to the presence of a TiO_2 barrier layer. Thus, the less active state achieved for nanotubular samples immersed in AS, may also be related to the formation of a passive oxide film with the ability to protect the Ti substrate against electrochemical attack. Interestingly, significantly higher OCP values were achieved after bio-functionalization treatments. In accordance with our previous work [56], beyond the fast and effective passivation ability, the bio-functionalized TiO_2 nanotubes are also expected to display a significantly lower passive current in AS compared to conventional nanotubes, most likely due to the presence of a nano-thick oxide film at the interface region (Fig. 2b). The oxide film grown during bio-functionalization treatments is expected to play a main role in corrosion, by restricting the movement of metal ions from the metallic surface to the surrounding medium [56].

Both groups of anodized Ti surfaces decorated with TiO_2 nanotubes present significantly higher OCP values before, during and after reciprocating sliding tests compared to Ti surfaces (Fig. 3a). It is known that the OCP recorded during sliding tests is a mixed potential reflecting the state of the unworn material and the state of the material in the wear track [16]. Garcia *et al.* [81] proposed the concept of active wear track area to investigate the wear-corrosion mechanisms of passive materials under sliding conditions. The active wear track area is defined as the part of the surface area that loses its passive film under mechanical loading, becoming activated electrochemically and suffering corrosion.

At the time the alumina ball is loaded on NT samples and the sliding starts, the OCP keeps stable for approximately 100 s (Fig. 3a and b – red curves). This behavior indicates that the electrochemical passive state of the material in the wear track keeps unaltered. Besides the running-in period observed during the first 100 s of sliding, the COF reaches a value of 0.6 after the first period of 60 s (Fig. 4b). This value is the one

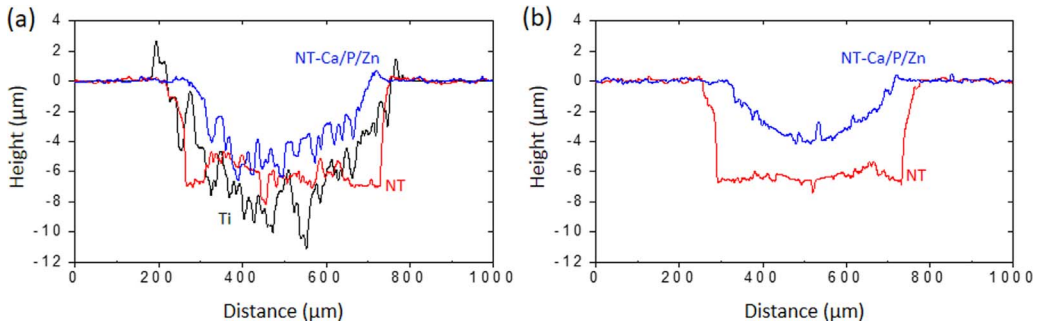

Fig. 11. 2D profiles obtained by profilometry in the central region of the wear tracks of Ti, NT and NT-Ca/P/Zn samples after sliding tests carried out for (a) 1800 and (b) 300 s. The tribo-electrochemical experiments were carried out in AS at a sliding frequency of 1 Hz, a load of 1 N and a displacement of 650 µm.

Table 1
Maximum depth of the wear tracks on Ti, NT and NT-Ca/P/Zn samples after 1800 s and 300 s sliding tests. The thickness of NT and NT-Ca/P/Zn films is also presented.

Group	Maximum wear track depth (µm)		Film thickness (µm)
	1800 s SLIDING	300 s SLIDING	
Ti	10.7 ± 0.4	–	–
NT	7.9 ± 0.9 *	8.3 ± 1.2	6.1 ± 0.1
NT-Ca/P/Zn	7.1 ± 0.4 *	4.1 ± 0.1 #	4.6 ± 0.1

* significantly different from Ti, $p < 0.05$.
\# significantly different from NT, $p < 0.05$.

expected for alumina/Ti oxide tribological pair, therefore indicating that the alumina ball is sliding against the TiO_2 nanotubular film. After this period of sliding, the OCP drops down (cathodic shift) suggesting that a more active state is achieved in the wear track, probably related to the detachment of the nanotubular film and the exposure of the metallic substrate to fresh electrolyte promoting corrosion. This may initiate a galvanic coupling between the passive surface and the bare Ti substrate, with consequent local dissolution of Ti [16]. For a better understanding of the OCP evolution during tribocorrosion, Vieira *et al.* [83] emphasized two different situations may happen: 1) the establishment of a galvanic coupling between the completely depassivated wear track and the surrounding passive area, or 2) a galvanic coupling within the wear track between depassivated and still passive areas [83]. Regarding NT samples the galvanic coupling is probably established according to the second case since, as the sliding goes on, the OCP slowly decreases indicating a gradual depassivation in the wear track area. In fact, after 1800 s of sliding, the nanotubular film is completely detached from the Ti substrate in the periphery of the contact area (Fig. 5b), however, the formation of a compacted oxide film is found in the contact region (Figs. 5b, 7b and 8a). As observed in Fig. 9a, the detachment of the film occurred during the first 300 s of sliding.

The morphology of the wear debris resulting from tribo-electrochemical degradation of conventional TiO_2 nanotubes is shown in Fig. 12a. From these SEM micrographs it is clearly observed that the main mechanisms assisting TiO_2 nanotubular film degradation are tube smashing and densification in the top region, accompanied by delamination and full detachment of the nanotubes, through cracks formation and propagation from the surface to subsurface regions of the film. These mechanisms are schematically illustrated in Fig. 13a. It is clearly observed that most of the wear debris are either single or aggregated nanotubes, coming from nanotube film break in different parts along the film length, resulting in fragments of the tubes with variable dimensions. The densification of the nanotubes accompanied by wear and fracture was also previously observed by nanoindentation studies [46,84]. Xu *et al.* [85] also studied the mechanical behavior of TiO_2 nanotube arrays by nanoindentation and observed that as the indentation depth increases the nanotubes break, interacting with neighboring nanotubes causing them to bend and fracture, with small fragments becoming compacted gradually, resulting in densification.

As a result of NT film detachment after 100 s of sliding, a large amount of film debris are released in the contact region, with part of them being either pushed out of the contact or becoming entrapped in it. As soon as the sliding goes on it is expected that the wear debris in the contact region are continuously exposed to mechanical and electrochemical solicitations, and several actions are prone to take place simultaneously or sequentially interacting with each other in a complex way. One of them is the formation a compact oxide film in the central region of the wear track as a result of the continuous smashing/densification of the film debris, as observed after 1800 s (Figs. 5b, 6d and 7b) and 300 s (Fig. 9a and c) sliding tests. The formation of this tribolayer may grant protection to the Ti substrate against corrosion and wear, and may explain both the COF and the gradual lowering of the OCP during sliding. A similar level of mechanical destruction of NT samples is observed after 300 s (Fig. 9a) and 1800 s (Fig. 5b) sliding tests. This suggests that after the catastrophic NT film degradation which takes place between 100 s and 300 s of sliding, the tribolayer formed in the contact region has the ability to protect the substrate against mechanical wear as long the sliding action takes place, as emphasized by the similar wear volumes measured after 300 s and 1800 s sliding tests (Fig. 10). Simultaneously to tribolayer formation, it is expected that during sliding some of the debris are pushed against the nanotubular film which is surrounding the sliding contact region, along with the counterbody movement. This probably induces to cyclic compressive stresses, which may lead to the progressive structural damage of surface and subsurface regions of the film, with formation and propagation of cracks and consequent delamination. This reveals the poor adhesion strength of TiO_2 nanotubes to the Ti substrate and its brittleness. Because of the brittle nature of TiO_2 nanotubes, they probably elastically bend up to very small strain and consequently, they collapse [85]. Signs of fatigue wear are visible through cracks on the nanotubular film surface outside the wear track (Fig. 6c). It is noteworthy that within crack formation and propagation the electrolyte may penetrate into the substrate inducing corrosion, which may further contribute to film detachment.

As previously mentioned, the OCP measured during sliding is a mixed potential reflecting the intrinsic potentials of the materials in active and passive areas. This may explain the minimum OCP measured during sliding on NT samples, which was around −0.3 V *vs.* SCE (Fig. 3a – red curve). It is expected that the large area of the Ti substrate exposed to AS in the periphery of the contact region, as a consequence of NT film detachment, together with the compacted oxide film formed in the sliding contact region, influence the OCP measurements. Furthermore, one must be highlighted that the area from where the nanotubular film was detached, is probably covered by a naturally formed passive film in AS, which is expected to influence the OCP measured. Once the sliding is stopped the OCP evolves slightly to higher values and does not reach the initial OCP back, indicating that repassivation takes place at a rather limited oxidation rate. The electrochemical state of the material in the worn area was irreversibly

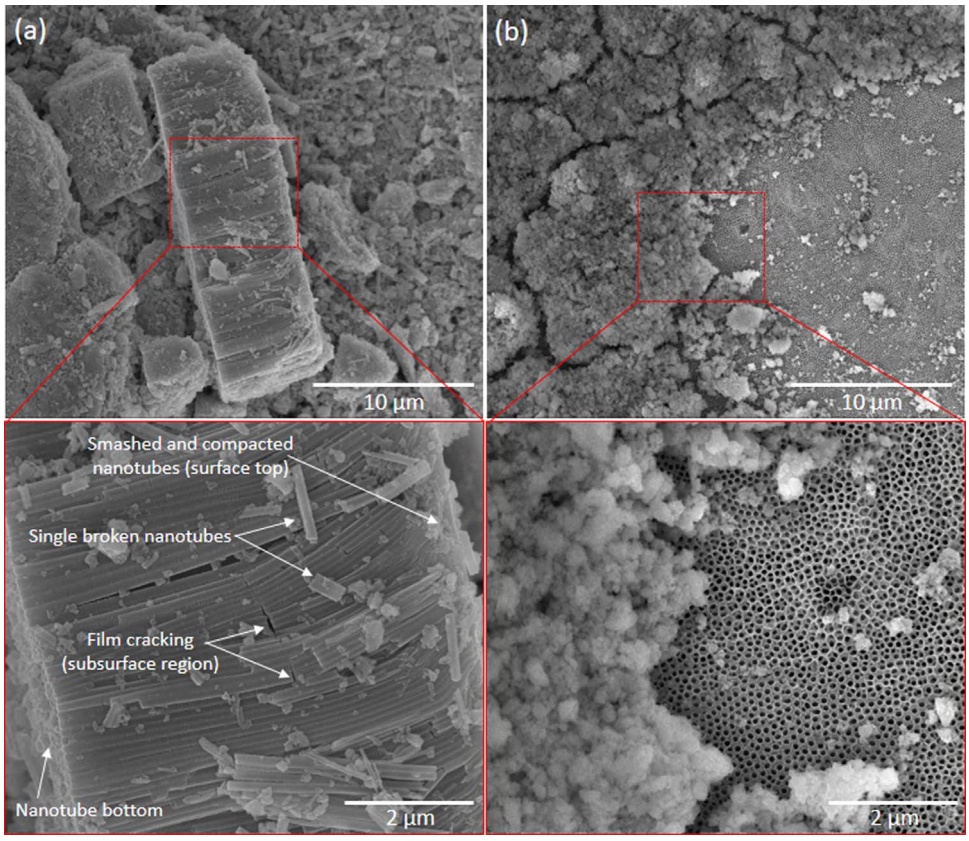

Fig. 12. SE SEM micrographs showing the wear debris morphology generated during tribo-electrochemical degradation of (a) NT and (b) NT-Ca/P/Zn samples.

modified as a consequence of sliding, with lower OCP values reflecting the more active electrochemical state of NT samples.

The tribo-electrochemical behavior of NT-Ca/P/Zn samples is significantly different compared to NT samples which may be both ascribed to the electrochemical and mechanical properties of the films as well to its adhesion strength to Ti substrate. After bio-functionalization treatments a nano-thick oxide film is formed at the interface of TiO_2 nanotubes (Fig. 2b). In addition, this may contribute to the less active electrochemical state (noble OCP) that bio-functionalized TiO_2 nanotubes exhibit during the whole duration of sliding, this also suggests that the contribution of corrosion reactions on their tribo-electrochemical degradation behavior is lower compared to Ti and NT films. However, additional studies should be performed to confirm this assumption.

The chemical features of NT-Ca/P/Zn surfaces may also influence their OCP values. In this work X-ray photoelectron spectroscopy (XPS) studies were carried out, from which the presence of Zn was detected on these surfaces and mostly assigned to ZnO compounds (results not shown). From observation of potential-pH diagram of Zn it is known that zinc oxides and hydroxides are soluble in acid media, which is accompanied by the release of Zn^{2+} ions that in equilibrium conditions have a standard potential of −0.762 V/NHE (Zn^{2+}/Zn) [86]. As the pH of AS at 37 °C is 5.5, it is expected that once NT-Ca/P/Zn samples are immersed in solution, the ZnO compounds are dissolved with formation of Zn^{2+} ions. This may explain the OCP drop in the beginning of mechanical solicitations and the fluctuations (cathodic shifts) registered along the sliding tests (Fig. 3a and b – blue curves). Beyond Zn, NT-Ca/P/Zn samples are also composed of Ca and P. From literature it is known that the corrosion resistance of Ti in simulating body fluids (pH = 7.4, 37 °C) is enhanced after deposition of a calcium phosphate layer

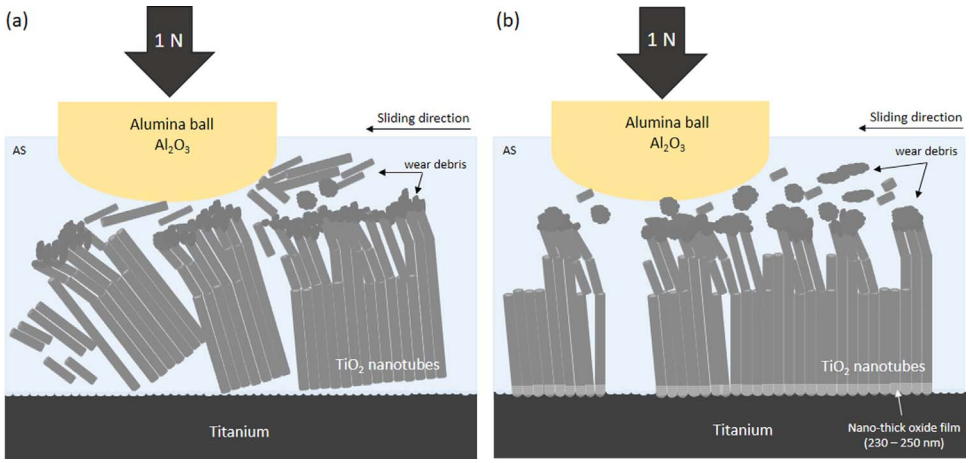

Fig. 13. Illustration of the tribo-electrochemical degradation mechanisms of TiO_2 nanotubes in (a) NT and (b) NT-Ca/P/Zn samples.

on its surface [87,88]. Additionally, Alves *et al.* [66] studied the tribocorrosion behavior of anodic films produced in an electrolyte containing β-glycerolphosphate and different concentrations of calcium acetate. The authors hypothesized that the reason for the improved tribocorrosion behavior of the anodic films, beyond the crystalline structure, could be the higher calcium content. Thus, it is believed that the Ca and P elements may have a beneficial effect on the tribo-electrochemical behavior of TiO_2 nanotubes, however, the underlying mechanisms are still unknown.

As soon as the mechanical solicitations starts, the OCP of NT-Ca/P/Zn samples drops and immediately after evolves to noble values reaching a steady state that is maintained during approximately 1000 s (Fig. 3a – blue curve). From sliding tests carried out for 300 s it is believed that the nanotubular film has not been fully detached out from the substrate during this first plateau, as suggested from SE and BSE images depicted in Fig. 9b and d. From wear track profiles shown in Fig. 11b it is confirmed the non-detachment of the film during the first 300 s of mechanical solicitations, since the maximum wear track depth is lower than the thickness of the film (Table 1) and significantly inferior to the maximum depth reached after 1800 s of sliding (Table 1). After 1000 s of sliding the OCP shifts down (cathodic shift) probably related to the detachment of the film with exposure of Ti substrate to the electrolyte, and thus achieving a more active state. As soon as the OCP decreases it is observed a slight decrease in the COF values (Fig. 4c), which may be related with film detachment. Afterwards, the OCP slightly increases as long as the sliding keeps on, which might be related to the filling of the nanotubes with film debris, accompanied by their continuous smashing and compactness in the sliding track creating a kind of a compact oxide film blocking the passage of the electrolyte and protecting the Ti substrate from the corrosive attack. This behavior may also indicate the repassivation ability of these samples as long as the sliding occurs.

From Fig. 7c and d it is observed that after 1800 s of sliding, the nanotubular film is organized in different layers in the wear track, which are found in different plans. In the topmost part, the nanotubes are not visible probably as a consequence of the successive mechanical solicitations as the rubbing action goes on. In the central region are visible some parts from where the fully detachment of the film took place, together with others where the nanotubes still maintain their integrity with well-opened pores. This suggests that the degradation of the film occurs gradually and by layers probably by a cracking-assisted mechanism. As a consequence of cyclic and compressive stresses induced on the surface and subsurface regions of the film, the nanotubes may crush and be smashed from the top to the inner regions. Cracks are visible along the wear track which may induce to film delamination. On the contrary to NT samples, the film cracking is restricted to the contact region and no detachment occurs in the vicinity of the worn area.

The morphology of the wear debris observed after tribo- electrochemical degradation of bio-functionalized TiO_2 nanotubes is remarkable different compared to the one observed for non-functionalized nanotubes, as shown in Fig. 12b. Most of the wear debris present smaller dimensions and a non-defined morphology probably as a result of the mechanical/electrochemical solicitations at which were imposed for a longer period of time, as a consequence of the improved adhesion strength of the film and its resistance to detach as long as the sliding takes place. Contrarily to NT samples, the mechanical degradation of NT-Ca/P/Zn samples seems to occur gradually. The main mechanisms assisting the tribo-electrochemical degradation of bio-functionalized TiO_2 nanotubes may be summarized as smashing and densification in the top region, with gradual detachment of the film by layers, through cracks formation and propagation from the top to the inner regions of the film. These mechanisms are schematically illustrated in Fig. 13b. The results above discussed are in good agreement with the significantly lower wear volume measured for bio-functionalized nanotubes both after 300 s and 1800 s of sliding compared to conventional TiO_2 nanotubes (Fig. 10).

Finally it is noteworthy to highlight that on unloading, the OCP of NT-Ca/P/Zn samples immediately starts to increase and reaches, after some time, the OCP achieved during the first 1000 s of sliding (Fig. 3a – blue curve). On the other hand, if the sliding is finished after 300 s, the OCP achieves the initial OCP back (Fig. 3b – blue curve). This suggests that if the nanotubular film is not completely detached during sliding, the material in the wear track has the ability of repassivation with the re-establishment of the initial surface passive state. However, once the nanotubular film peels off and comes out of the substrate, the passive state achieved in the first 1000 s of sliding is re-established instead of the initial one. This behavior shows the very strong repassivation ability of bio-functionalized nanotubes even when the nanotubular film is detached, suggesting that the higher OCP of these samples is related to the existence of the nano-thick oxide film at the interface.

4.3. Limitations of the present study

As an innovative study, some limitations have been encountered. In this work, no information on the rate of the corrosion reactions neither on the synergism between wear and corrosion processes is provided. Therefore, further studies must be conducted to quantify the corrosion current released during mechanical solicitations, or even in their absence by potentiodynamic polarization studies. In order to better understand the tribo-electrochemical behavior of the nanotubular systems and their long-term stability, further studies should be performed for longer durations and multiple cycles of sliding, intended to mimic the multiple periods of mechanical solicitations that dental implants might be daily exposed. Furthermore, as future work it would be of upmost importance to investigate the mechanical properties of the TiO_2 nanotubes, before and after bio-functionalization. The information of the Young's modulus and hardness of the films must be addressed to understand their influence on the tribo-electrochemical degradation behavior of the films. Beyond the improved tribo-electrochemical behavior of bio-functionalized nanotubes when compared to Ti and conventional nanotubes, a considerable amount of wear debris is still released during tribo-electrochemical solicitations (Fig. 12). In the future, it would be interesting to study the osteoblasts ability to internalize the wear particles released by tribocorrosion, as well as their toxicity potential. Furthermore, additional surface functionalization techniques should be explored to improve the tribocorrosion resistance of the bio-functionalized nanotubular systems addressed in this work.

5. Conclusions

The tribo-electrochemical behavior of TiO_2 nanotubes before and after bio-functionalization treatments was investigated by reciprocating sliding tests carried out in artificial saliva. The tribo-electrochemical behavior of bio-functionalized TiO_2 nanotubes was significantly improved both from the electrochemical and the mechanical point of view. Hereafter follows the main outcomes of this study:

1. The electrochemical stability of TiO_2 nanotubes is enhanced after bio-functionalization treatments, displaying a less active state during the whole duration of tribo-electrochemical tests.
2. Bio-functionalized TiO_2 nanotubes display improved wear resistance, with the ability to withstand mechanical solicitations during 1000 s without fully film detachment.
3. The improved tribo-electrochemical behavior of bio-functionalized nanotubes is granted by the nano-thick oxide film grown at Ti/TiO_2 nanotubes interface, which concedes electrochemical stability and improves the adhesion strength of the film to Ti substrate, resulting in a reduced wear volume loss.
4. A first insight on the main degradation mechanisms of TiO_2 nanotubular films was proposed which relies on tube smashing

and densification, accompanied by delamination and detachment of the tubes, through cracks formation and propagation from the surface to subsurface regions of the film.

This investigation provides, for the first time, new knowledge on the main degradation mechanisms of TiO_2 nanotubes before and after bio-functionalization treatments. The methodology adopted for nanotubes functionalization, based on reverse polarization and anodization treatments, shows up as a very simple and effective way to create a multifunctional nano-thick oxide film at the interface region. This film has the ability to protect the Ti substrate against the simultaneous action of electrochemical and mechanical solicitations, by enhancing the adhesion strength of the film to the substrate. This comes out as a very promising methodology to improve the long term biomechanical stability of TiO_2 nanotubes for osseointegrated implants applications.

Acknowledgements

This work was supported by FCT with the reference project UID/EEA/04436/2013 and by FEDER funds through the COMPETE 2020 – Programa Operacional Competitividade e Internacionalização (POCI) with the reference project POCI-01–0145-FEDER-006941.

The authors also acknowledge the financial support from FCT by the doctoral grant (Ref. SFRH/BD/88517/2012), CAPES (Proc. 99999.008666/2014-08), CNPq (Proc. 490761/2013-5) and UNESP. Also, the authors would like to thank LABNANO/CBPF (Brazilian Center for Research in Physics) for all the support in electron microscopy analyses. Tolou Shokuhfar is especially thankful to US National Science Foundation NSF-DMR CAREER award # 1564950.

References

[1] M. Niinomi, Mechanical properties of biomedical titanium alloys, Mater. Sci. Eng.: A 243 (1998) 231–236.
[2] Y. Oshida, E.B. Tuna, O. Aktören, K. Gençay, Dental implant systems, Int. J. Mol. Sci. 11 (2010) 1580–1678.
[3] I. Demetrescu, C. Pirvu, V. Mitran, Effect of nano-topographical features of Ti/TiO2 electrode surface on cell response and electrochemical stability in artificial saliva, Bioelectrochemistry 79 (2010) 122–129.
[4] C. Yao, E.B. Slamovich, T.J. Webster, Enhanced osteoblast functions on anodized titanium with nanotube-like structures, J. Biomed. Mater. Res. A 85 (2008) 157–166.
[5] W.-E. Yang, M.-L. Hsu, M.-C. Lin, Z.-H. Chen, L.-K. Chen, H.-H. Huang, Nano/submicron-scale TiO_2 network on titanium surface for dental implant application, J. Alloy. Compd. 479 (2009) 642–647.
[6] M.C. Garcia-Alonso, L. Saldana, G. Valles, J.L. Gonzalez-Carrasco, J. Gonzalez-Cabrero, M.E. Martinez, E. Gil-Garay, L. Munuera, In vitro corrosion behaviour and osteoblast response of thermally oxidised Ti_6Al_4V alloy, Biomaterials 24 (2003) 19–26.
[7] B.I. Johansson, B. Bergman, Corrosion of titanium and amalgam couples: effect of fluoride, area size, surface preparation and fabrication procedures, Dent. Mater. 11 (1995) 41–46.
[8] G. Manivasagam, D. Dhinasekaran, A. Rajamanickam, Biomedical implants: corrosion and its prevention - a review, recent patents on, Corros. Sci. 2 (2010) 40–54.
[9] A.C. Vieira, A.R. Ribeiro, L.A. Rocha, J.P. Celis, Influence of pH and corrosion inhibitors on the tribocorrosion of titanium in artificial saliva, Wear 261 (2006) 994–1001.
[10] L. Ceschini, E. Lanzoni, C. Martini, D. Prandstraller, G. Sambogna, Comparison of dry sliding friction and wear of Ti6Al4V alloy treated by plasma electrolytic oxidation and PVD coating, Wear 264 (2008) 86–95.
[11] A.L. Yerokhin, A. Leyland, A. Matthews, Kinetic aspects of aluminium titanate layer formation on titanium alloys by plasma electrolytic oxidation, Appl. Surf. Sci. 200 (2002) 172–184.
[12] A.F. Yetim, Investigation of wear behavior of titanium oxide films, produced by anodic oxidation, on commercially pure titanium in vacuum conditions, Surf. Coat. Technol. 205 (2010) 1757–1763.
[13] J. Souza, S. Barbosa, E. Ariza, J.-P. Celis, L. Rocha, Simultaneous degradation by corrosion and wear of titanium in artificial saliva containing fluorides, Wear 292 (2012) 82–88.
[14] F.G. Oliveira, A.R. Ribeiro, G. Perez, B.S. Archanjo, C.P. Gouvea, J.R. Araújo, A.P. Campos, A. Kuznetsov, C.M. Almeida, et al., Understanding growth mechanisms and tribocorrosion behaviour of porous TiO^2 anodic films containing calcium, phosphorous and magnesium, Appl. Surf. Sci. 341 (2015) 1–12.
[15] R.J. Wood, Tribo-corrosion of coatings: a review, J. Phys. D: Appl. Phys. 40 (2007) 5502.
[16] P. Ponthiaux, F. Wenger, D. Drees, J.-P. Celis, Electrochemical techniques for studying tribocorrosion processes, Wear 256 (2004) 459–468.
[17] S.B. Goodman, Wear particles, periprosthetic osteolysis and the immune system, Biomaterials 28 (2007) 5044–5048.
[18] N. Cobelli, B. Scharf, G.M. Crisi, J. Hardin, L. Santambrogio, Mediators of the inflammatory response to joint replacement devices, Nat. Rev. Rheumatol. 7 (2011) 600–608.
[19] A.R. Ribeiro, S. Gemini-Piperni, R. Travassos, L. Lemgruber, R. C. Silva, A.L. Rossi, M. Farina, K. Anselme, T. Shokuhfar, et al., Trojan-like internalization of anatase titanium dioxide nanoparticles by human osteoblast cells, Sci. Rep. 6 (2016) 23615.
[20] M. Sampaio, M. Buciumeanu, B. Henriques, F.S. Silva, J.C.M. Souza, J.R. Gomes, Tribocorrosion behavior of veneering biomedical PEEK to Ti6Al4V structures, J. Mech. Behav. Biomed. Mater. 54 (2016) 123–130.
[21] F. Toptan, A. Rego, A.C. Alves, A. Guedes, Corrosion and tribocorrosion behavior of Ti–B4C composite intended for orthopaedic implants, J. Mech. Behav. Biomed. Mater. 61 (2016) 152–163.
[22] F. Toptan, A.C. Alves, A.M.P. Pinto, P. Ponthiaux, Tribocorrosion behavior of bio-functionalized highly porous titanium, J. Mech. Behav. Biomed. Mater. 69 (2017) 144–152.
[23] M. Buciumeanu, A. Araujo, O. Carvalho, G. Miranda, J.C.M. Souza, F.S. Silva, B. Henriques, Study of the tribocorrosion behaviour of Ti_6Al_4V–HA biocomposites, Tribol. Int. 107 (2017) 77–84.
[24] V. Gopal, M. Chandran, M.S.R. Rao, S. Mischler, S. Cao, G. Manivasagam, Tribocorrosion and electrochemical behaviour of nanocrystalline diamond coated Ti based alloys for orthopaedic application, Tribol. Int. 106 (2017) 88–100.
[25] I. Hacisalihoglu, A. Samancioglu, F. Yildiz, G. Purcek, A. Alsaran, Tribocorrosion properties of different type titanium alloys in simulated body fluid, Wear 332–333 (2015) 679–686.
[26] D.R.N. Correa, P.A.B. Kuroda, C.R. Grandini, L.A. Rocha, F.G.M. Oliveira, A.C. Alves, F. Toptan, Tribocorrosion behavior of β-type Ti-15Zr-based alloys, Mater. Lett. 179 (2016) 118–121.
[27] V.G. Pina, V. Amigó, A.I. Muñoz, Microstructural, electrochemical and tribo-electrochemical characterisation of titanium-copper biomedical alloys, Corros. Sci. 109 (2016) 115–125.
[28] Marques IdSV, M.F. Alfaro, M.T. Saito, N.C. da Cruz, C. Takoudis, R. Landers, M.F. Mesquita, F.H. Nociti Junior, M.T. Mathew, et al., Biomimetic coatings enhance tribocorrosion behavior and cell responses of commercially pure titanium surfaces, Biointerphases 11 (2016) 031008.
[29] J. Villanueva, L. Trino, J. Thomas, D. Bijukumar, D. Royhman, M.M. Stack, M.T. Mathew, Corrosion, tribology, and tribocorrosion research in biomedical implants: progressive trend in the published literature, J. Bio- Tribo-Corros. 3 (2017) 1.
[30] A.P. Tomsia, M.E. Launey, J.S. Lee, M.H. Mankani, U.G. Wegst, E. Saiz, Nanotechnology approaches for better dental implants, Int. J. Oral Maxillofac. Implants 26 (2011) 25.
[31] S. Oh, C. Daraio, L.-H. Chen, T.R. Pisanic, R.R. Fiñones, S. Jin, Significantly accelerated osteoblast cell growth on aligned TiO_2 nanotubes, J. Biomed. Mater. Res. A 78A (2006) 97–103.
[32] K.S. Brammer, C.J. Frandsen, S. Jin, TiO_2 nanotubes for bone regeneration, Trends Biotechnol. 30 (2012) 315–322.
[33] L. Zhao, H. Wang, K. Huo, L. Cui, W. Zhang, H. Ni, Y. Zhang, Z. Wu, P.K. Chu, Antibacterial nano-structured titania coating incorporated with silver nanoparticles, Biomaterials 32 (2011) 5706–5716.
[34] K.S. Brammer, S. Oh, C.J. Cobb, L.M. Bjursten, H. van der Heyde, S. Jin, Improved bone-forming functionality on diameter-controlled TiO2 nanotube surface, Acta Biomater. 5 (2009) 3215–3223.
[35] K. Das, S. Bose, A. Bandyopadhyay, TiO_2 nanotubes on Ti: influence of nanoscale morphology on bone cell–materials interaction, J. Biomed. Mater. Res. Part A 90 (2009) 225–237.
[36] T. Shokuhfar, A. Hamlekhan, J.-Y. Chang, C.K. Choi, C. Sukotjo, C. Friedrich, Biophysical evaluation of cells on nanotubular surfaces: the effects of atomic ordering and chemistry, Int. J. Nanomed. 9 (2014) 3737.
[37] J. Lellouche, E. Kahana, S. Elias, A. Gedanken, E. Banin, Antibiofilm activity of nanosized magnesium fluoride, Biomaterials 30 (2009) 5969–5978.
[38] J. Liao, M. Anchun, Z. Zhu, Y. Quan, Antibacterial titanium plate deposited by silver nanoparticles exhibits cell compatibility, Int. J. Nanomed. 5 (2010) 337–342.
[39] H.L. Cao, X.Y. Liu, F.H. Meng, P.K. Chu, Biological actions of silver nanoparticles embedded in titanium controlled by micro-galvanic effects, Biomaterials 32 (2011) 693–705.
[40] M.A. Vargas-Reus, K. Memarzadeh, J. Huang, G.G. Ren, R.P. Allaker, Antimicrobial activity of nanoparticulate metal oxides against peri-implantitis pathogens, Int. J. Antimicrob. Agents 40 (2012) 135–139.
[41] F. Al-Hazmi, F. Alnowaiser, A.A. Al-Ghamdi, A.A. Al-Ghamdi, M.M. Aly, R.M. Al-Tuwirqi, F. El-Tantawy, A new large – Scale synthesis of magnesium oxide nanowires: structural and antibacterial properties, Superlattices Microstruct. 52 (2012) 200–209.
[42] J. Lellouche, A. Friedman, J.-P. Lellouche, A. Gedanken, E. Banin, Improved antibacterial and antibiofilm activity of magnesium fluoride nanoparticles obtained by water-based ultrasound chemistry, Nanomed.: Nanotechnol. Biol. Med. 8 (2012) 702–711.
[43] C. Moseke, F. Hage, E. Vorndran, U. Gbureck, TiO_2 nanotube arrays deposited on Ti substrate by anodic oxidation and their potential as a long-term drug delivery system for antimicrobial agents, Appl. Surf. Sci. 258 (2012) 5399–5404.
[44] B. Ercan, E. Taylor, E. Alpaslan, T.J. Webster, Diameter of titanium nanotubes influences anti-bacterial efficacy, Nanotechnology 22 (2011) 295102.
[45] Y. Zhao, Q. Xing, J. Janjanam, K. He, F. Long, K.-B. Low, A. Tiwari, F. Zhao, R. Shahbazian-Yassar, et al., Facile electrochemical synthesis of antimicrobial TiO_2

nanotube arrays, Int. J. Nanomed. 9 (2014) 5177.
[46] G. Crawford, N. Chawla, K. Das, S. Bose, A. Bandyopadhyay, Microstructure and deformation behavior of biocompatible TiO_2 nanotubes on titanium substrate, Acta Biomater. 3 (2007) 359–367.
[47] J.-Y. Rho, T.Y. Tsui, G.M. Pharr, Elastic properties of human cortical and trabecular lamellar bone measured by nanoindentation, Biomaterials 18 (1997) 1325–1330.
[48] P. Soares, A. Mikowski, C.M. Lepienski, E. Santos, G.A. Soares, N.K. Kuromoto, Hardness and elastic modulus of TiO_2 anodic films measured by instrumented indentation, J. Biomed. Mater. Res. B: Appl. Biomater. 84 (2008) 524–530.
[49] T. Shokuhfar, G.K. Arumugam, P.A. Heiden, R.S. Yassar, C. Friedrich, Direct compressive measurements of individual titanium dioxide nanotubes, ACS Nano 3 (2009) 3098–3102.
[50] Y. Hu, K.Y. Cai, Z. Luo, D.W. Xu, D.C. Xie, Y.R. Huang, W.H. Yang, P. Liu, TiO_2 nanotubes as drug nanoreservoirs for the regulation of mobility and differentiation of mesenchymal stem cells, Acta Biomater. 8 (2012) 439–448.
[51] M.L. Macdonald, R.E. Samuel, N.J. Shah, R.F. Padera, Y.M. Beben, P.T. Hammond, Tissue integration of growth factor-eluting layer-by-layer polyelectrolyte multilayer coated implants, Biomaterials 32 (2011) 1446–1453.
[52] D.-W. Lee, Y.-P. Yun, K. Park, S.E. Kim, Gentamicin and bone morphogenic protein-2 (BMP-2)-delivering heparinized-titanium implant with enhanced antibacterial activity and osteointegration, Bone 50 (2012) 974–982.
[53] K. Gulati, S. Ramakrishnan, M.S. Aw, G.J. Atkins, D.M. Findlay, D. Losic, Biocompatible polymer coating of titania nanotube arrays for improved drug elution and osteoblast adhesion, Acta Biomater. 8 (2012) 449–456.
[54] K.C. Popat, M. Eltgroth, T.J. LaTempa, C.A. Grimes, T.A. Desai, Decreased Staphylococcus epidermis adhesion and increased osteoblast functionality on antibiotic-loaded titania nanotubes, Biomaterials 28 (2007) 4880–4888.
[55] H. Hu, W. Zhang, Y. Qiao, X. Jiang, X. Liu, C. Ding, Antibacterial activity and increased bone marrow stem cell functions of Zn-incorporated TiO_2 coatings on titanium, Acta Biomater. 8 (2012) 904–915.
[56] S.A. Alves, S.B. Patel, C. Sukotjo, M.T. Mathew, P.N. Filho, J.-P. Celis, L.A. Rocha, T. Shokuhfar, Synthesis of calcium-phosphorous doped TiO_2 nanotubes by anodization and reverse polarization: a promising strategy for an efficient biofunctional implant surface, Appl. Surf. Sci. 399 (2017) 682–701.
[57] T. Fusayama, T. Katayori, S. Nomoto, Corrosion of gold and amalgam placed in contact with each other, J. Dent. Res. 42 (1963) 1183–1197.
[58] S. Alves, R. Bayón, A. Igartua, V. Saénz de Viteri, L. Rocha, Tribocorrosion behaviour of anodic titanium oxide films produced by plasma electrolytic oxidation for dental implants, Lubr. Sci. 26 (2014) 500–513.
[59] S. Alves, R. Bayón, V.S. de Viteri, M. Garcia, A. Igartua, M. Fernandes, L. Rocha, Tribocorrosion behavior of calcium-and phosphorous-enriched titanium oxide films and study of osteoblast interactions for dental implants, J. Bio- Tribo-Corros. 1 (2015) 1–21.
[60] A. Robin, J. Meirelis, Influence of fluoride concentration and pH on corrosion behavior of Ti-6Al-4V and Ti-23Ta alloys in artificial saliva, Mater. Corros. 58 (2007) 173–180.
[61] J.C. Souza, S.L. Barbosa, E.A. Ariza, M. Henriques, W. Teughels, P. Ponthiaux, J.-P. Celis, L.A. Rocha, How do titanium and Ti_6Al_4V corrode in fluoridated medium as found in the oral cavity? An in vitro study, Mater. Sci. Eng.: C 47 (2015) 384–393.
[62] R. Holland, Corrosion testing by potentiodynamic polarization in various electrolytes, Dent. Mater. 8 (1992) 241–245.
[63] L. Benea, E. Mardare-Danaila, J.-P. Celis, Increasing the tribological performances of Ti–6Al–4V alloy by forming a thin nanoporous TiO_2 layer and hydroxyapatite electrodeposition under lubricated conditions, Tribol. Int. 78 (2014) 168–175.
[64] M.J. Runa, M.T. Mathew, M.H. Fernandes, L.A. Rocha, First insight on the impact of an osteoblastic layer on the bio-tribocorrosion performance of Ti_6Al_4V hip implants, Acta Biomater. 12 (2015) 341–351.
[65] M. Runa, M. Mathew, L. Rocha, Tribocorrosion response of the Ti6Al4V alloys commonly used in femoral stems, Tribol. Int. 68 (2013) 85–93.
[66] A. Alves, F. Oliveira, F. Wenger, P. Ponthiaux, J.-P. Celis, L. Rocha, Tribocorrosion behaviour of anodic treated titanium surfaces intended for dental implants, J. Phys. D: Appl. Phys. 46 (2013) 404001.
[67] M.T. Mathew, S. Abbey, N.J. Hallab, D.J. Hall, C. Sukotjo, M.A. Wimmer, Influence of pH on the tribocorrosion behavior of CpTi in the oral environment: synergistic interactions of wear and corrosion, J. Biomed. Mater. Res. B: Appl. Biomater. 100 (2012) 1662–1671.
[68] A. Butt, N.B. Lucchiari, D. Royhman, M.J. Runa, M.T. Mathew, C. Sukotjo, C.G. Takoudis, Design, development, and testing of a compact tribocorrosion apparatus for biomedical applications, J. Bio-Tribo-Corros. 1 (2015) 4.
[69] H.V. Cruz, J.C.M. Souza, M. Henriques, L.A. Rocha, Tribocorrosion and bio-tribocorrosion in the oral environment: the case of dental implants, in: J.P. David (Ed.), Biomedical Tribology, Nova Science Publishers, 2011, pp. 1–30.
[70] Z. Doni, A. Alves, F. Toptan, J. Gomes, A. Ramalho, M. Buciumeanu, L. Palaghian, F. Silva, Dry sliding and tribocorrosion behaviour of hot pressed CoCrMo biomedical alloy as compared with the cast CoCrMo and Ti_6Al_4V alloys, Mater. Des. 52 (2013) 47–57.
[71] W.-q Yu, J. Qiu, L. Xu, F.-q Zhang, Corrosion behaviors of TiO_2 nanotube layers on titanium in Hank's solution, Biomed. Mater. 4 (2009) 065012.
[72] W.-q Yu, J. Qiu, F.-q Zhang, In vitro corrosion study of different TiO_2 nanotube layers on titanium in solution with serum proteins, Colloids Surf. B: Biointerfaces 84 (2011) 400–405.
[73] N. Diomidis, J.P. Celis, P. Ponthiaux, F. Wenger, A methodology for the assessment of the tribocorrosion of passivating metallic materials, Lubr. Sci. 21 (2009) 53–67.
[74] T. Hanawa, K. Asami, K. Asaoka, Repassivation of titanium and surface oxide film regenerated in simulated bioliquid, J. Biomed. Mater. Res. 40 (1998) 530–538.
[75] Id.S.V. Marques, M.F. Alfaro, N.C. da Cruz, M.F. Mesquita, C. Sukotjo, M.T. Mathew, Barão VAR, Tribocorrosion behavior of biofunctional titanium oxide films produced by micro-arc oxidation: synergism and mechanisms, J. Mech. Behav. Biomed. Mater. 60 (2016) 8–21.
[76] P. Roy, S. Berger, P. Schmuki, TiO_2 nanotubes: synthesis and applications, Angew. Chem. Int. Ed. 50 (2011) 2904–2939.
[77] G. Ali, C. Chen, S.H. Yoo, J.M. Kum, S.O. Cho, Fabrication of complete titania nanoporous structures via electrochemical anodization of Ti, Nanoscale Res. Lett. 6 (2011) 1–10.
[78] X. Yuan, M. Zheng, L. Ma, W. Shen, High-speed growth of TiO_2 nanotube arrays with gradient pore diameter and ultrathin tube wall under high-field anodization, Nanotechnology 21 (2010) 405302.
[79] D. Wang, B. Yu, C. Wang, F. Zhou, W. Liu, A novel protocol toward perfect alignment of anodized TiO_2 nanotubes, Adv. Mater. 21 (2009) 1964–1967.
[80] R. Beutner, J. Michael, B. Schwenzer, D. Scharnweber, Biological nano-functionalization of titanium-based biomaterial surfaces: a flexible toolbox, J. R. Soc. Interface 7 (2010) S93–S105.
[81] I. Garcıa, D. Drees, J.-P. Celis, Corrosion-wear of passivating materials in sliding contacts based on a concept of active wear track area, Wear 249 (2001) 452–460.
[82] J. Grotberg, A. Hamlekhan, A. Butt, S. Patel, D. Royhman, T. Shokuhfar, C. Sukotjo, C. Takoudis, M.T. Mathew, Thermally oxidized titania nanotubes enhance the corrosion resistance of Ti_6Al_4V, Mater. Sci. Eng.: C 59 (2016) 677–689.
[83] A.C. Vieira, L.A. Rocha, N. Papageorgiou, S. Mischler, Mechanical and electrochemical deterioration mechanisms in the tribocorrosion of Al alloys in NaCl and in $NaNO_3$ solutions, Corros. Sci. 54 (2012) 26–35.
[84] G. Crawford, N. Chawla, J. Houston, Nanomechanics of biocompatible TiO_2 nanotubes by interfacial force microscopy (IFM), J. Mech. Behav. Biomed. Mater. 2 (2009) 580–587.
[85] Y. Xu, M. Liu, M. Wang, A. Oloyede, J. Bell, C. Yan, Nanoindentation study of the mechanical behavior of TiO_2 nanotube arrays, J. Appl. Phys. 118 (2015) 145301.
[86] P. Delahay, M. Pourbaix, P. Van Rysselberghe, Potential-pH diagram of zinc and its applications to the study of zinc corrosion, J. Electrochem. Soc. 98 (1951) 101–105.
[87] K. Indira, U. Kamachi Mudali, N. Rajendran, Corrosion behavior of electrochemically assembled nanoporous titania for biomedical applications, Ceram. Int. 39 (2013) 959–967.
[88] X. Cheng, S.G. Roscoe, Corrosion behavior of titanium in the presence of calcium phosphate and serum proteins, Biomaterials 26 (2005) 7350–7356.